Development of an automated pipeline to search for solar system objects in TRAPPIST data

Auteur : Sicorello, Guillaume
Promoteur(s) : Jehin, Emmanuel
Faculté : Faculté des Sciences
Diplôme : Master en sciences spatiales, à finalité approfondie
Année académique : 2019-2020
URI/URL : http://hdl.handle.net/2268.2/9956

University of Liège

Faculty of Sciences

Department of Astrophysics, Geophysics and Oceanography

Master thesis

Development of an automated pipeline to search for solar system objects in TRAPPIST data

A thesis presented for the degree of Master in Space Sciences by

Guillaume Sicorello

Under the supervision of Emmanuel Jehin

Academic Year 2019–2020

Remerciements

J'adresse mes premiers remerciements à Emmanuel Jehin, pour m'avoir admis dans son service et permis de travailler sur les données des télescopes TRAPPIST et SPECULOOS. Par sa passion du métier, j'ai beaucoup appris sur le monde des petits corps.

Je remercie également Sandrine Sohy pour ses nombreux conseils en matière de programmation et Marin Ferrais pour m'avoir épaulé durant la réalisation de ce mémoire.

Merci également à Max Mahlke pour avoir patiemment répondu à toutes mes questions concernant l'outil `ssos` .

Sur un plan plus personnel, je souhaiterais remercier ma maman, ma sœur ainsi que toute ma famille pour le soutien qu'ils m'ont apporté. Je remercie aussi mes amis, Ben, Jean, Antoine, Joséphine, Svetlana, Lucas, et tous les autres, pour m'avoir si souvent fait oublier le temps qui passe.

Contents

Acronyms

AU	Astronomical Unit
CSS	Catalina Sky Survey
DEC	Declination
FITS	Flexible Image Transport System
GAIA DR2	Gaia Data Release 2
IAU	International Astronomical Union
IRAF	Image Reduction and Analysis Facility
MPC	Minor Planet Center
NEO	Near-Earth Object
Pan-STARRS	Panoramic Survey Telescope and Rapid Response System
PHA	Potentially Hazardous Asteroid
RA	Right Ascension
SCAMP	Software for Calibrating AstroMetry and Photometry
SExtractor	Source-Extractor
SkyBoT	Sky Body Tracker
SSO	Solar System Object
TNO	Trans-Neptunian Object
TRAPPIST	TRAnsiting Planets and PlanetesImals Small Telescope
WCS	World Coordinate System

Chapter 1

Introduction

Today, we know that our solar system is only one expression of a common feature in the Universe. This same Universe seems to be full of exoplanets orbiting around one or several stars in a more or less elliptical journey. Only change the configuration of the system, the numbers and the type of the star(s), the number, the size and the type of the planet(s) and, in our case, the presence of life on one of them. Recently, our solar system was even visited by interstellar smaller objects like the asteroid 1I/2017 U1 ('Oumuamua) (Meech et al., 2017) and the comet 2I/Borisov (Guzik et al., 2019), ejected from their own planetary system a long time ago. Their detections prove that even these smaller bodies are common outside our system.

Nevertheless, regardless of its prevalent nature, our solar system appears to be quite rich and complex if we take a closer look. It is made up of a G2V star, four rocky planets, four gaseous and icy giant planets, five dwarf planets, more than one hundred and fifty moons and millions of small solar system objects (or small bodies). This last group is made up of a large variety of bodies(Near-Earth Objects, Main-Belt asteroids, Jupiter family comets, Centaurs, Kuiper-belt Objects, Oort cloud comes) which differ in mass and composition and are present in all the solar system.

These small bodies are the remnant of the formation of our system. Some of these objects like the comets have barely changed since the collapse of the early solar nebula and hold important clues of its primary composition, physical conditions and dynamics. Other small bodies are the by-product of collisions between planetesimals, like it is the case for Main-Belt asteroids, and from their composition and orbit we can learn more about the solar system history.

Small bodies could also have played a role in the development of life. Even if we are still unsure of the way it occurred, we know that the Earth was hit at a high rate by asteroids or comets about 3.9 billions years ago. It is referred as the Late Heavy Bombardment (Lowe and Byerly, 2018). Some geochemical indicators show that life could have already existed on Earth more than 3.7 billions years ago (Rosing and Frei, 2004). From these conclusions, several studies argue that this bombardment could have brought either a lot of organic molecules used for life or a sufficient amount of energy to synthesize these building blocks from abiotic elements present in the atmosphere or in the ocean (Chyba and Sagan, 1992).

Ironically, some of these small bodies constitute today a threat for life on Earth.

It is for example the case for asteroids, referred as Near-Earth Asteroids, whose orbits can cross the one of the Earth, leading to a risk of collision. It is likely that such an event caused the extinction of the dinosaurs 66 million years ago. It is thus imperative to discover a maximum of these hazardous objects, especially the ones larger than 100 m, and precisely compute their orbits in order to prevent a potential disaster in the future.

Discovering small solar system objects

For all these reasons, the small bodies are actively studied through in-situ measurements, in space and from the ground. Since the discovery of (1) Ceres in 1801, millions of observations lead to the detection of more than 963,000 small bodies[1]. However, a lot of small bodies are yet to be discovered and we always need observations to precise even more the orbit of the already-known ones. The number of discoveries has exploded the last 10 years with new surveys dedicated to monitor the sky, to search for hazardous small bodies.

The Panoramic Survey Telescope and Rapid Response System (Pan-STARRS) (Kaiser et al., 2010; Chambers et al., 2016) is one of these sky tracker. It is constituted of two 1.8m class telescopes, located at Haleakala Observatories on the island of Maui, in the Pacific and operated by the Institute for Astronomy at the University of Hawaii. Since 2014, the Pan-STARRS facility is mainly dedicated to the search and detection of NEOs in the context of the NASA NEO Observations program (Wainscoat et al., 2015). Up to now, the telescopes have discovered more than 5000 Near-Earth Objects (NEOs) ans more than 300 Potentially Hazardous Asteroids (PHAs). It is notably one of the Pan-STARRS telescopes that discovered the asteroid 1I/2017 U1 ('Oumuamua). This large number of detections is mainly due to the Image Processing Pipeline, a dedicated software used by Pan-STARRS to process its images and found a maximum of moving targets in it.

Another survey that search for NEOs is the Catalina Sky Survey (CSS)[2]. Funded by NASA as part of the Near Earth Object Observation Program, the CSS is composed of three 1.5m, 1m and 0.7m class telescopes, operated by the Lunar and Planetary Lab of the University of Arizona. Its main goal is to discover a maximum of NEOs with a size equal or larger than 140 m. With Pan-STARRS, it is the project that discovered the greatest numbers of NEOs. Once again, CSS rely on sophisticated detection software in order to retrieve a maximum of moving objects in its images fields.

Apart from these missions fully dedicated to the detection of small bodies of the solar system, various facilities that pursue other goals do not necessarily have all the computer background to automatically tracks down moving targets in the images. In addition, the software computer code of these big survey are private and cannot be shared. Yet, there are a lot of archival images from various projects that are a gold mine for finding small bodies and that would needs to be searched for with optimised and dedicated tools. In particular, it is the case for the TRAPPIST

---

[1]https://minorplanetcenter.net/mpc/summary
[2]https://catalina.lpl.arizona.edu/about

and SPECULOOS telescopes, lead by teams of the university of Liège. Moving objects are often caught in these observations, crossing the field-of view and recorded by the CCD cameras. If they are found and identified, these objects could be studied for "free", by measuring their precise positions and brightness. In term of observation nights, there are about 300 good nights per year in Chile and 250 in Tenerife and Morocco. Together, multiplied by the years of activity of each telescope, that represents since the starts of the projects about 5250 nights. Knowing that between 500 and 1000 images are taken per night, the telescopes databases contain already 2,5 millions images only for TRAPPIST-south telescope in 10 years of observations. These images could contain thousands of wanderer small bodies to be measured.

Scientific motivation

The main goal of this work is to implement a suits of programs, referred as the `automated SSOS` pipeline, that is optimised to find moving objects and can be included in the dataflow to automatically search the data when they are taken at the telescope or after the night is over. Our pipeline is based on a new software package, the `ssos` tool (Mahlke et al., 2019), that has been adapted to our needs and optimised for the TRAPPIST and SPECULOOS projects.

The development and implementation of this pipeline is driven by a set of scientific goals. The main goal is to retrieve the lightcurves of hundreds of asteroids. Indeed a lot of asteroids are expected to be present in the archival images of TRAPPIST and SPECULOOS and it would be valuable to find them.

Due to the asteroids irregular shapes, their rotation produce light variations with time. These flux variations can be recorded in lightcurves, built from their photometric measurements in each image. With a sufficiently long time baseline, these lightcurves can be used to deduce the rotation periods of the asteroids. For most asteroids, the rotation period is comprised between 2.4 and 24 hours Warner et al. (2009) while for TRAPPIST and SPECULOOS telescopes, in the context of the programs of exoplanets, can stay on one or two fields for up to 20 nights, allowing very long baseline. These archival data are then very well suited to find rotation periods still not measured for a lot of asteroids.

Some asteroids are slow rotators with rotation periods that can be as long as several days. These asteroids are very poorly studied as their rotation is so slow, and it would be interesting to find more of them and to see if there is any bias in this population (Marciniak et al., 2015). With the very long time series that we should get on the objects detected in these data sets, we could have a better statistics on their occurrence and maybe find some clues about their peculiarity. For asteroids at the opposition and moving very slowly on the sky, such measurements should be possible and we could track them during a maximum number of nights.

The survey of asteroid lightcurves could also reveal very fast rotators (Monteiro et al., 2020) which are also quite rare and very interesting to set up the limit between the rubble pile[3] and single rocky body limit for asteroids. Indeed the 2.4 hours limit

---

[3]Asteroid with a diameter between 200 m and 10 km, that are mainly composed of objects

is usually the fasted rotation that can sustain an asteroid before breaking up due to the balance between internal strength and the centripetal force.

This sample should hopefully reveal also a bunch of new binaries as there are about 15% of asteroids which are couples (Margot et al., 2015). These asteroids are very interesting as thanks to their orbital period their masses can be derived which is usually very difficult to get for an asteroid.

An other use of such data, for an extended observing period providing lightcurves taken at different phase angles, allow to derive the precise shape of the asteroid after 3D shape reconstruction (Kaasalainen et al., 2002; Durech et al., 2009).

The precise astrometric measurements of all the objects detected by the pipeline will be submitted to the Minor Planet Center (MPC) and will be used to compute more precise orbits. It is particularly important for the NEOs or PHAs, whose orbits need to be precisely computed in order to check well in advance a possible collision with the Earth (Ivantsov et al., 2019). Astrometric measurements are also of great importance regarding the comets as their orbits slightly change with time, perturbed by non-gravitational effect like the outgassing.

Finally, the pipeline could lead to the discovery of new asteroids, and maybe if we are lucky, as they are more rare, new comets, large Trans-Neptunian Objects (TNOs) or even interstellar objects, recorded in the images by chance. There are dedicated surveys that are doing such searches every clear nights, but still a serendipitous discovery is always possible as the telescope just needs to point at the right place at the right moment. As TRAPPIST and SPECULOOS are looking any location in the sky, and not specifically the ecliptic, it is possible to find interesting objects on high inclination orbits that have escaped detection until today. In addition, the pipeline could once again play a preventive role with regard to the risk of a collision with the Earth. Indeed, more than 90% of NEOs larger than 1 km have been discovered but there are still a lot of observations to perform to recover those with a size smalled 140 m[4].

Work plan

In addition to the introduction and the conclusion, this work is divided into five chapters.

In chapter 2, general information is provided. We review the definition and the different classes of small bodies in the solar system. A few words are given about the way of naming small bodies.

In chapter 3, a description of the TRAPPIST and SPECULOOS telescopes is presented.

In chapter 4, the calibration process is described as well as the photometry and astrometry. The calibration process is first presented, with a description of the bias, dark and flat-field steps. Then the implemented scripts to calibrate a large number of images are explained. After that, we depict the photometry and astrometry processes.

(rubble) linked together by the gravitational force (Walsh, 2018)

[4]Minimal size for an object to be considered as hazardous

In chapter 5, the software chosen to implement the search in the TRAPPIST and SPECULOOS images, the so-called the `ssos` tool, is presented. We describe the way it works, the various steps and sub-routines as well as the different parameters used. The search for the best parameters to optimise `ssos` is also presented.

In chapter 6, the `automated SSOS` pipeline itself, developed in this work, and the first results are presented.

Chapter 2

The world of small bodies

As this work is about the small bodies of the solar system, this first chapter is dedicated to their presentation. First we define them and we present the different classes of small bodies, according to their distances to the Sun. Then, as the program developed in this work could lead to discoveries of new celestial objects, the way of naming them is explained.

2.1   Definition

All the celestial bodies in the solar system can be organised into four categories: planets, dwarf planets, satellites and small bodies. The definitions of each of these categories are set by the International Astronomical Union (IAU). The most recent definitions were voted by the IAU in 2006[1]. As a reminder, a planet must fulfill three criteria:

(i) A planet orbits the Sun.

(ii) A planet is sufficiently massive to reach a hydrostatic equilibrium.

(iii) A planet has cleared the neighbourhood of it orbit.

From these criteria, we can deduce the definitions of a dwarf planet and a small body. A dwarf planet does not fulfill the third criterium:

(i) A dwarf planet orbits the Sun.

(ii) A dwarf planet is sufficiently massive to assume a hydrostatic equilibrium.

(iii) A dwarf planet has not cleared the neighbourhood of its orbit.

(iv) A dwarf planet is not a satellite.

The last criterium is needed to avoid any confusion and overlapping between the different categories. Concerning the small bodies, they are defined as followings:

(i) A small body orbits the Sun.

---

[1] https://www.iau.org/news/pressreleases/detail/iau0602/

(ii) A small body is not sufficiently massive to assume a hydrostatic equilibrium.

(iii) A small body has not cleared the neighbourhood of its orbit.

(iv) A small body is not a satellite.

In other words, a celestial body belonging to our solar system is referred as a small body if it is neither a planet, a dwarf planet or a satellite.

2.2 The various classes of small bodies

Small bodies differ in size, composition and location around the Sun. If we put aside the smallest (dust particles and meteorites), the two main classes of small bodies are certainly the asteroids and the comets.

An asteroid can be defined as a rocky, carbonaceous or metallic small body that, a priori, shows no detectable outflow of gas or dust (Spohn et al., 2014; NASA/JPL, a). Its size can vary from a few meters to about one thousand of kilometers[2]. Most of the asteroids are located between Mars and Jupiter in the so-called main asteroid belt. However to a lesser extend, they are present everywhere in the system. Trojans, Centaurs, TNOs are examples of other groups of asteroids, organised following their orbit around the Sun. We can also mention the Near-Earth Asteroids as part of the NEO groups, defined after their close approach to the Earth orbit (semi major axis a < 1,3 au) and for which they constitute a potential hazard.

Comets are small rocky bodies that contain a large fraction of ices. If their orbit bring them close to the Sun, the ices melt and release the dust and molecules previously trapped in it, leading to the formation of the typical comet coma (Spohn et al., 2014; NASA/JPL, b). Usually, the size of the nucleus of a comet does not exceed a few kilometers. Their high content in ice indicates that they problably originate from the outer part of the solar system, beyond the orbit of Neptune. However, comets can also cross the inner solar system if their orbits have been perturbed by the giant planets gravity or collisions.

Nevertheless, these two classes seem to mingle more and more as our knowledge concerning the small bodies of the solar system increases. As an example representing the difficulty to distinguish the two groups, recent discoveries indicate that some asteroids can become active and show a certain comet-like outgassing (Jewitt, 2012) and might form a new class, the main belt comets, and/or be just activated asteroids.

The amount of small bodies presents in the inner and outer part of the solar system is illustrated in figure 2.1.

---

[2](1) Ceres was the largest asteroid until 2006 with a diameter of 946 km.

<div align="center">
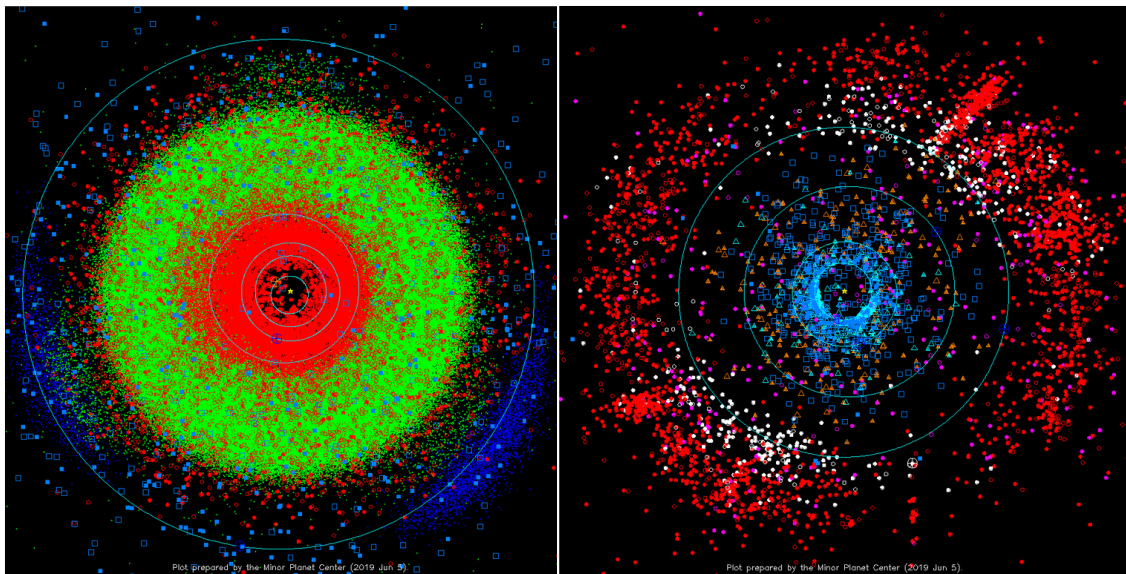
Inner solar system.   Outer solar system.

</div>

Figure 2.1: These plots represent the positions at a certain time of most of the known small bodies displayed in the inner or outer parts of the solar system. The large light blue circles represent the orbits of the planets. The colored circles, triangles or dots represent the asteroids and the colored squares represent the comets. A filled or unfilled circle or triangle is linked to the number of observations at the opposition. Concerning the comets, the filled squares represent the numbered (i.e. permanently designated) periodic comets and the empty squares represent the other comets. The colors are linked to the orbital parameters of the asteroids. On the inner solar system image, the red circles and the blue dots are respectively the asteroids with a perihelium within 1.3 au and the trojan asteroids of Jupiter. The green dots are the other asteroids and delimit very well the main asteroid belt. On the outer solar system image, cyan and orange triangles respectively show objects with a high eccentricity and the Centaur objects. The white and magenta circles respectively show plutoids, scattered disk objects. The red circles are other objects (Minor Planet Center, 2019a,b).

2.2.1   The Asteroids

Most of the asteroids are located in the main asteroid belt which extends from 2.2 au up to 3.28 au from the Sun. Studies based on observations and albedo/absolute magnitude show that there are between 1.1 million and 1.9 million kilometer-sized asteroids and millions of smaller ones (O'Brien and Greenberg, 2005; Tedesco and Desert, 2002). These objects are thought to be the remnants of disruptive collisions between planetesimals. At this place of the solar system, the formation of a planet could have been inhibited by the large gravitational interaction with Jupiter. Inside the main belt, there are forbidden semi major axes due to resonances between Mars and Jupiter. These resonances are called the Kirkwood gaps and are responsible for the ejection of asteroids towards the inner solar system, and are then the origin of the Near-Earth Asteroids population, that can cross the Earth orbit.

Another well-known group of asteroids are the Trojans. They stay around the stable lagrangian points L_4 and L_5 of some of the planets, especially Jupiter. Today,

the most common theory to explain their origin is the capture of TNO after they were scattered inward the solar system due to the migration of the giant planets according to the Nice model and Grand Tack models, at the early stage of the solar system (Emery et al., 2015). Up to now, 8596 are known[3].

Farther out in the solar system, the Centaurs population include the small icy bodies orbiting between Saturn and Uranus and the ones orbiting beyond Saturn and crossing the orbit of one of the planet. They are far from the Sun and the large majority of them are inactive, but a few of them are showing some cometary activity. Their nature is still uncertain, which is the origin of their name. They probably come from the Kuiper Belt. The Centaurs are on non stable orbits and are expected to be ejected from the solar system.

Finally, small and large icy asteroids are also present beyond the orbit of Neptune as part of the TNOs population. For most of them, their orbit would have been more or less deeply perturbed during the migration of the giant planets in the early stages of the solar system (Pike et al., 2017). It resulted in the existence of two TNO populations, referred as the cold and the hot populations. The former one, is made up of small bodies that have been less perturbed by the migration and have a low eccentricity and inclination. In the latter population, they have high eccentricities and inclinations (up to several tens of degree). As a consequence, the area beyond Neptune is often divided into two regions, namely the Kuiper Belt and the scattered disk. The Kuiper Belt is a region that extends between about 30 au (Neptune's orbit) and 50 au. It mainly contains cold population objects and a few of the hot population ones. At the contrary, the scattered disk is completely depleted in cold population bodies. It extends from the outer part of the Kuiper Belt up to approximately 1,000 au.

2.2.2 The Comets

The comets originate from the outer part of the solar system. They orbit around the Sun as part of the Kuiper belt, the scattered disk or the Oort cloud[4]. The comets with an orbit that bring them close to the Sun are classified in several ways. Following the semi-major axis and orbital period, comets with periods lower or larger than 200 years are respectively called short-period or long-period comets. The short-period ones are also divided in two well known groups: the Halley-type comets (P > 20 years) and the Jupiter-Family comets (P < 20 years). The orbits of these comets are not very much inclined with respect to the ecliptic plane and are often called ecliptic comets. The long-period comets, depending on the value of their semi-major axes, are called returning comets (if a < 10,000 years) or new comets (if a > 10,000 years) if they come for the first time close to the Sun. Contrarily to the ecliptic comets, their orbits can be very inclined, and retrograde, coming isotropically from any direction.

---

[3]https://minorplanetcenter.net/mpc/summary
[4]The Oort Cloud is a spherical reservoir at about 1 light year and centred on the Sun

2.2.3   The Near-Earth Objects

The NEOs are defined by a perihelion distance smaller than 1.3 au. They have been formerly ejected from their orbits by some gravitational or collisional interactions and now wander across the inner solar system. As illustrated in table 2.1, they are spread into different groups in function of their nature or their orbital parameters.

Group	Semi-major axis (a)	Perihelion distance (q)	Aphelion distance (Q)
Amor	1 au < a	1.017 au < q < 1.3 au	No constraint
Apollo	1 au < a	1.017 au > q	No constraint
Aten	1 au > a	No constraint	0.983 au < Q
Atira	1 au > a	No constraint	0.983 au > Q
Group	**MOID**	**Absolute magnitude (H)**	
PHA	MOID $\leqslant$ 0.05 au	H $\leqslant$ 22	

Table 2.1: The different groups of NEOs (NASA/JPL Center for Near Earth Object Studies). MOID and PHA stand respectively for Minimum Orbit Intersection Distance (with the Earth) and Potential Hazardous Asteroid. The absolute magnitude H is directly linked to the size of the NEO. For an albedo of 0.3, an absolute magnitude of 22 corresponds to an object with a size close to 100 m.

As seen in figure 2.2, the number of known NEOs exceeds today 23,000 objects. The NEOs are very interesting objects to study because their regular close approach allows to observe them from close and to gather unique informations, like to resolve the shape and the surface of the asteroid which is not possible for distant asteroids. As some of them are crossing the Earth orbit and could potentially hit the Earth, they are also subject to a close monitoring by spatial administrations.
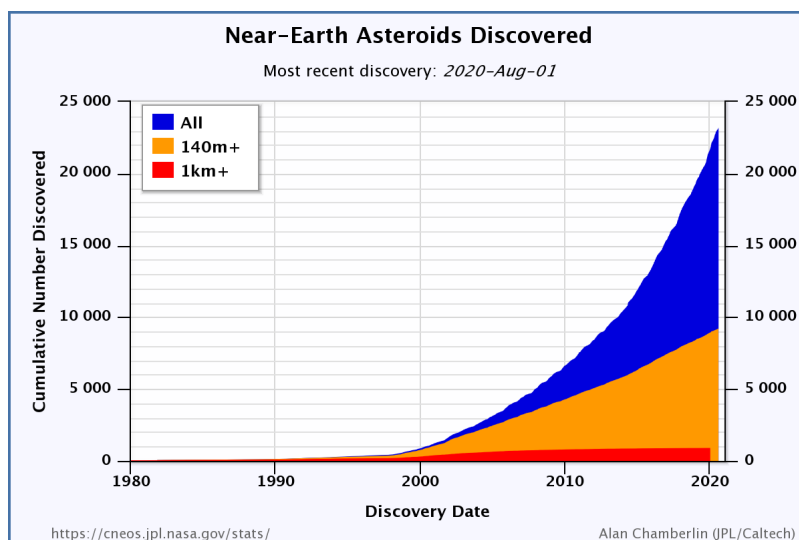

Figure 2.2: The number of discovered NEOs with time (NASA/JPL Center for Near Earth Object Studies, 2020).

2.3 Naming minor planets and comets

As the heart of this work consists of developing a pipeline that could lead to the detection of still unknown SSOs, it could be useful to explain the way of naming them.

Naming celestial objects is the task of the IAU and its Divisions[5]. In the case of small bodies, this task is done by the MPC, a part of the IAU. The MPC is entirely dedicated to the identification and the orbit computation of small bodies[6]. To do so, the MPC relies on position measurements made by astronomers all around the world. Any discovery of unknown objects or tracking of already-known object can be reported to the MPC. When the discovery of a new object is attributed to someone, that person has the privilege to chose a name for it.

2.3.1 Naming a minor planet

A minor planet is a non-cometary small body. A provisional designation is given to any minor planet observed during two different nights without being identified with an already-known object[7]. This temporary name is of the canonical form $\mathbf{\Lambda\Lambda\Lambda\Lambda\ \Omega\Omega_\Lambda}$, with $\mathbf{\Lambda}$ representing digits and $\mathbf{\Omega}$ representing upper case letters. The four first digits $\mathbf{\Lambda\Lambda\Lambda\Lambda}$ represent the year of discovery. The first of the two capitals letters $\mathbf{\Omega}$ corresponds to the part of the month the major planet was discovered (A: 1-15 Jan., B: 16-31 Jan.,...; the letters I and Z are omitted). The second capital letter $\mathbf{\Omega}$ displays the rank of the minor planet in the list of discoveries (A: 1$^{\text{st}}$, B: 2$^{\text{nd}}$,...; the letter I is omitted). The subscripted digit $\mathbf{\Lambda}$ of $\mathbf{\Omega_\Lambda}$ only appears if more than 25 minor planets are discovered during one single part of a month. In that case, the alphabet is recycled and an index beginning by 1 is added to the nomenclature. As an example, the minor planet $\mathbf{1999\ CU_3}$ is a small body discovered during the first part of February in 1999. If U stands for the 20$^{\text{th}}$, it is the $25 \times 3 + 20\ = 95^{\text{th}}$ discovery within that part of the month.

This style of provisional designation was set up from the start of the year 1925. Before, the way minor planets were designated was a little bit chaotic. The very first discovered small bodies were referred by names. In the beginning of the 1850s, new discoveries began to be designated by a number instead of a name but it was not until 1892 that the year of discovery was used in the designation. After that, the identification style changes several times as the number of discovered objects grew. Between 1892 and 1925, one or two upper or lower case letter(s) were employed in addition to the year of discovery. Greek letters have even been used during world war one. Therefore, it was decided to extend the post-1925 provisional designation style to pre-1925 discoveries. The way of working is quite the same except that the letter $\mathbf{A}$ replaces the first digit of the date. As an example, the first minor planet discovered in the first half of May 1907 will receive the name $\mathbf{A907\ JA}$ as provisional designation.

---

[5]https://www.iau.org/public/themes/naming/#minorplanets

[6]In addition to the different groups of small bodies already mentioned in the above section, the MPC is also in charge of the irregular satellites of the major planets.

[7]https://minorplanetcenter.net//iau/info/OldDesDoc.html

After having observed a minor planet so many times that its orbit is well determined (in fact it needs to be observed at three different oppositions), the MPC assigns a number to it, which represents its permanent designation. From this point, the person who discovered the minor planet can suggest a name[8] within a period of ten years[9]. The name needs to be approved by the Working Group for Small Body Nomenclature of the IAU.

2.3.2 Naming a comet

Comets receive also a provisional and permanent designations. Since 1995, the provisional designation is of the kind $\Omega/\Lambda\Lambda\Lambda\Lambda \; \Omega\Lambda$, with the same legend as for the minor planets. The letter Ω used as a prefix is linked to the nature of the comet. It can have five values: **P** for a periodic comet; **C** for a non-periodic comet; **X** if we do not know if the comet is periodic or not; **D** if the comet no longer exists and **I** if the comet comes from interstellar space. The set of four digits $\Omega/\Lambda\Lambda\Lambda\Lambda$ represents the year of discovery. Concerning the two last symbols, the capital letter Ω represents the part of the month the comet was discovered and uses the same capital letters as for minor planets and the digit Λ is the rank of the comet in the list of the discoveries during the part of the month. Contrarily to the minor planets, a comet automatically receives the names of their discoverers (maximum two names) and is used as part of the designation. The names is chosen in agreement with both the MPC and the Working Group for Small Body Nomenclature. As an example, the comet **C/2006 P1 (McNaught)** is the first non periodic comet discovered in the first part of August in 2006 by Robert H. McNaught.

When a comet appears in the sky for the second time, the MPC gives it a permanent number which represents the rank of the comet among all the discovered comets in the concerned class (P, C, X, D, I). The name is used both with the provisional designation and with the permanent designation. For example, **1P/Halley** is the first periodic comet ever observed and it was discovered by Edmond Halley.

---

[8]The list of minor planet names: https://minorplanetcenter.net//iau/lists/MPNames.html

[9]Witch is the only way to name a small body. It is notably impossible to buy a name.

Chapter 3

The TRAPPIST and SPECULOOS telescopes

This chapter describes the TRAPPIST and SPECULOOS telescopes for which the `automated SSOS` pipeline was built. After a description of the telescopes properties and the dataflow, we detail the advantages of the pipeline with regard to the telescopes observingq strategies. Finally, we examine the apparent small bodies velocities for various classes of objects.

3.1 TRAPPIST

The TRAnsiting Planets and PlanetesImals Small Telescopes (TRAPPIST)[1] (Jehin et al., 2011) are two 60cm class robotic Ritchey-Chretien telescopes that are operated by the Origins in Cosmology and Astrophysics group at the Department of Astrophysics, Geophysics and Oceanography of the University of Liège (Belgium). The first TRAPPIST telescope, renamed TRAPPIST-South, was installed at La Silla Observatory[2] in Chile and started its observations in June 2010. The second telescope, TRAPPIST-North, was installed in the other hemisphere at the Oukaïmeden Observatory in Morocco and began its operations in October 2016.

The TRAPPIST observation program is divided into two main activities. About 50% of the telescope time is dedicated to the study of exoplanets through the transit method. Exoplanetary targets can be either exoplanet candidates or confirmed exoplanets. In the case of a candidate, TRAPPIST tends to confirm (or reject) its planetary nature through new transit observations. If it is an already confirmed cases, its observation aims to constrain even more its orbital and physical parameters. The TRAPPIST telescopes are notably well-known thanks to the discovery of a planetary system made up of seven Earth-like exoplanets orbiting close to their host star, a bright ultra-cool dwarfs star, TRAPPIST-1 (Gillon et al., 2017).

The other 50% of the time is devoted to the observation of comets, through the study of their chemical composition and their activity along their orbits, and to the observation of other small bodies. TRAPPIST observations contributed to

---

[1] https://www.trappist.uliege.be/
[2] https://www.eso.org/public/teles-instr/lasilla/trappist/

Figure 3.1: TRAPPIST-North (left picture) and TRAPPIST-South (right picture) telescopes (crédit E. Jehin).

the discovery of two dust rings surrounding the asteroid (10199) Chariklo (Braga-Ribas et al., 2014). These rings were discovered as the asteroid was passing in front of a star. The same occultation method involving TRAPPIST observations also highlighted some discoveries about the size and the atmosphere of the dwarf planets Eris and Makemake (Sicardy et al., 2011; Ortiz et al., 2012). From these observations, it appears today that Eris has almost the same size as Pluto and Makemake seems deprived of an atmosphere.

TRAPPIST-South and North

As we mainly worked with TRAPPIST-South data, we present here a more detailed description of the telescope. By its location, TRAPPIST-South is enable to perform high quality observation. The telescope is located in the Atacama desert in Chile, in the la Silla Observatory, one of the best place in the world to observe the sky.

TRAPPIST-South is equipped with a 2048×2048 CCD camera with a pixel scale of 0.64"/pixel and covering a field of view of about $22' \times 22'$. The camera offers the possibility to combine and read pixels four by four (binning 2) instead of one by one (binning 1). Although this procedure reduces the resolution, it increases the sensitivity of the detection and are particularly useful to observe the faintest sources. The camera has also three different readout mode[3]: 1×1 MHz, 1×2 MHz and 2×2 MHz. In this work, we only use images recorded with the 1×1 MHz mode (readout mode 1) and the 2×2 MHz mode (readout mode 2).

The telescopes are also equipped with two filter wheels, containing 7 broad and 11 narrow band filters. The broad-band filters are mainly used to study the asteroids and the exoplanets. In details, the telescope uses the Johnson-Cousins B, V, R_c, I_c and Sloan z filters that cover a wavelength range between 360 nm and 1100 nm, the Exo filter that cuts the blue light beyond 500 nm and the near infra-red I+z' filter for observations at a wavelength above 700 nm and that is mostly used for the TRAPPIST ultra cool dwarf exoplanet survey. The narrow band filters are used to detect the reflected or emitted light of a specific species and are more dedicated to the study of the composition of comets atmospheres. The filter wheel is loaded with

---

[3]read speed of the readout electronic

OH, NH, CN, CO$^+$,C$_3$, BC (Blue Continuum), C$_2$, GC (Green Continuum), RC (Red Continuum), NaI and H$_2$O$^+$ filters built by NASA (Farnham et al., 2000).

On table 3.1, we list the main characteristics of TRAPPIST-South. In order to give a comparison, the TRAPPIST-North characteristics are also given. The telescope is exactly the same but the camera CCD is of an other brand with a pixel size slightly smaller.

	TRAPPIST-South	TRAPPIST-North
Site	La Silla Observatory (I40)	Oukaïmeden Observatory (Z53)
Altitude (m)	2315	2751
Latitude	29° 15′ 16.6″ (S) / 29.2546° (S)	31° 12′ 22″ (N) /31.2061° (N)
Longitude	70° 44′ 121.8″ (W) / 70.7394° (W)	7° 51′ 29″ (W) / 7.8664° (W)
Diameter Primary (m)	0.6	
Mount	Model: Astelco NTM-500 - Type: German equatorial	
Camera model	FLI ProLine PL3041-BB	Andor IKONL BEX2 DD
Array size (pixels)	2048×2048	2048×2048
Pixel scale (arcsecs/pixels)	0.64	0.60
Field of view	22′×22′	20′×20′
Broad band filters	B, V, Rc, Ic, Sloan z, I+z', Exo, NaI, H$_2$O$^+$	B, V, Rc, Ic, Sloan z, Exo, NaI
Narrow band filters	OH, NH, CN, C$_3$, CO$^+$, BC, C$_2$, GC, RC	OH, NH, CN, C$_3$, Hα, BC, C$_2$, GC, RC

Table 3.1: Characteristics of TRAPPIST-South and TRAPPIST-North.

3.2 SPECULOOS

The Search for habitable Planets EClipsing ULtra-cOOL Stars (SPECULOOS) (Delrez et al., 2018; Burdanov et al., 2018; Jehin et al., 2018) project, is based on five 1m class robotic telescopes. Four of these telescopes constitute the SPECULOOS Southern Observatory and are located at Cerro Paranal, in Chile. The observatory was inaugurated in December 2019. The last one is located in the Instituto de Astrofísica de Canarias, in Tenerife and is operated by the Massachusetts Institute of Technology, the University of Liège, and the Institute of Astrophysics of the Canaries. With a total mirror area four times larger than TRAPPIST, SPECULOOS telescopes can detect objects down to a magnitude of about 21, compared to about 19 for TRAPPIST. On table 3.2, we list the main characteristics of SPECULOOS.
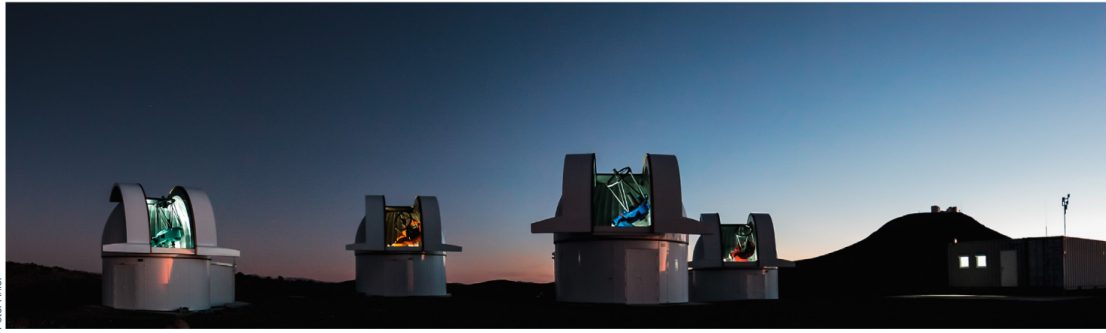
Figure 3.2: The four SPECULOOS telescopes located at Cerro Paranal, in Chile (Jehin et al., 2018).

The entire observation time of the SPECULOOS telescopes are dedicated to the search of exoplanets in the habitable zone around close ultra-cool dwarf stars. These stars are prime targets as the exoplanets in the habitable zone orbit in only a few days around their stars and they produced relatively deep transits (Gillon, 2018).

	SPECULOOS Southern Observatory	SPECULOOS Northern Observatory
Site	Cerro Paranal (W75)	Teide Observatory (954)
Altitude (m)	2518	2390
Latitude	24° 36′ 57.9″ (S)	28° 18′ 0″ (N)
Longitude	70° 23′ 25.8″ (W)	16° 30′ 35″ (W)
Diameter Primary (m)	4 x 1	1 x 1
Telescope	Astelco RC Lightweight Telescope - Ritchey-Chretien - F/8	
Mount	Model: Astelco NTM-1000 - Type: German equatorial	
Camera model	Andor iKon-L	
Array size (pixel)	2048×2048	
Pixel scale (arcsecs/pixel)	0.35	
Field of view	12′×12′	

Table 3.2: Characteristics of the SPECULOOS network.

3.3 Dataflow

When an image is taken with the telescope it is written on the local computer disk with a FITS header containing a large set of keywords written by the telescope software (like the name of the image, the UT time the image was taken, the exposure time used, the filter,...). A special script is then ran to made the FITS headers compatible with the ESO archive[4] images FITS headers. The astrometry is performed using the Astrometry.net engine[5] and World Coordinates are written in the fits headers (WCS). All the images as well as the calibrations frames are then transferred around noon every day to the local TRAPPIST and SPECULOOS archives in Liège and to ESO archive in Garching. Our pipeline is installed on an independent machine in the TRAPPIST control room in Liège that receives a copy of the new data. As soon as the transfer is completed, the pipeline starts automatically the

---

[4]http://archive.eso.org/
[5]http://astrometry.net/

data reduction and search of moving objects. The list of objects found is then ready in the end of the afternoon to be examined by the telescope operator.

The images produced are in the Flexible Image Transport System (FITS) format, a widely used format in astronomy. In addition to the observation image, this format notably allows the transport of metadata, like the properties of the image and telescope used, often referred as the FITS header. Just after the observations, the astrometry is performed on the images.

3.4 Observing strategy

The TRAPPIST and SPECULOOS observing strategy regarding the exoplanets surveys suits very well the creation of a pipeline to detect moving objects. The telescopes exposure time is between 15 and 60 seconds most of the time, providing between 500 and 2000 images per night in average. For most of the nights usually only one to two different fields are observed. In addition, the telescopes observe the same field during 10 to 20 nights, providing very long photometric series between 100 and 200 hours on the same field. Solar system objects with a sufficiently low velocity can then be tracked by the pipeline many hours per night and from even night to night.

The large amount of astrometric and photometric measurements that can be collected by the pipeline, thanks to these multiple-nights track is very interesting to characterise the asteroid rotation as explained before. Indeed, the precise rotation period of an asteroid can only be computed from a lightcurve covering several rotations. For asteroids with a long rotation period, their observation during several nights is also the only way to cover a complete lightcurve. For asteroids with a very short rotation period, it is possible to cover even several periods in only one night. The rotation period is then found using time-series analysis methods. However, the resulting period lacks accuracy and there is a risk that multiple period values (aliases) fit the data as well. In order to reduce the uncertainty and the number of aliases, multiple-night observations are required. Observing an asteroid on consecutive nights can help to reduce the number of aliases.

The TRAPPIST and SPECULOOS targets are observed at any position in the sky and not only near the ecliptic plane. As a consequence, we should be able to find highly inclined small bodies, usually missed by "classic" surveys. These kind of surveys mainly monitor the sky close to the ecliptic plane in order to find a maximum of small bodies (mostly main belt asteroids).

3.5 Small bodies apparent velocity

As the small bodies are located at sometimes very different distances from the Earth and move in different relative directions, their apparent velocities (i.e. their projected displacement rates on the sky) greatly differ from each other. As a consequence, the pipeline detection strategy has to take these information into account to not miss some of these objects.

Population	TRAPPIST-South (hour)	TRAPPIST-North (hour)	SPECULOOS (hour)
NEA	$30.5^{-13.9}_{+25.9}$	$27.7^{-12.7}_{+23.6}$	$16.6^{-7.6}_{+14.1}$
MC	$32^{-11.3}_{+18}$	$29^{-10.3}_{+16.4}$	$17.4^{-6.2}_{+9.8}$
MB	$40.6^{-7.9}_{+8.3}$	$37^{-7.2}_{+7.6}$	$22.2^{-4.3}_{+4.5}$
Trojan	$99.2^{-9.5}_{+8.9}$	$90.2^{-8.6}_{+8.1}$	$54.1^{-5.1}_{+4.9}$
Centaur	$330^{-138.7}_{+198}$	$1200^{-1026.1}_{+720}$	$720^{-615.7}_{+432}$
KBO	$2200^{-733.3}_{+440}$	$2000^{-666.7}_{+400}$	1200^{-400}_{+240}
Comet	$300^{-174.5}_{+207.7}$	$272.7^{-159.5}_{+188.8}$	$163.6^{-95.7}_{+113.3}$

Table 3.3: Table indicating the time needed for each population to cross the field of view side-to-side, for TRAPPIST and SPECULOOS. The field of view of TRAPPIST-South, TRAPPIST-North and SPECULOOS are respectively 22'×22', 20'×20' and 12'×12'.

An estimation of the velocity for different categories of small bodies is given in figure 3.3.

Population	Rate ($''$/h)
NEA	$43.3^{+36.5}_{-19.9}$
MC	$41.3^{+22.6}_{-14.9}$
MB	$32.5^{+7.9}_{-5.5}$
Trojan	$13.3^{+1.4}_{-1.1}$
Centaur	$4.0^{+2.9}_{-1.5}$
KBO	$0.6^{+0.3}_{-0.1}$
Comet	$4.4^{+6.2}_{-1.8}$

Figure 3.3: Velocity estimations for different small bodies categories (Carry, 2017). The rate column contains the apparent velocities on the sky of different groups of small bodies. Next to the values are also written the 25% and 75% quartile variations. Hence, the velocity ranges stand for half the population. For comets and NEA it is clear that the velocities can vary a lot depending on the distance to the Earth. NEA stands for Near Earth Asteroids, MC stands for Mars-Crosser, MB stands for Main-Belt Asteroids and KBO stands for Kuiper Belt Objects. Trojan are satellites that are orbiting the Sun on the same orbit as Jupiter and located 60 deg before or after the planet, Centaurs are objects between comets and asteroids and orbiting in the region of the giant planets.

It is possible to roughly compute the crossing time of a small body through an observed field. On Table 3.3 we estimated the time to cross the field of view side-to-side of the TRAPPIST and SPECULOOS telescopes.

In all the categories, some objects can stay more than one night in the same field. The KBO, the Comets and some Centaurs could even have the possibility to be tracked during all the observation duration of a given field by SPECULOOS and TRAPPIST. Note that for asteroids close to the opposition, the time can also be very long as they are nearly stationary on the sky.

We can also compute the time needed for the different populations to produce a displacement of the order of the seeing (typically 1.5"). It is particularly useful if we need to stack the images. If we stack images on a too long period, the small bodies appear in the form of trails and will be harder to recover. The time corresponding to a displacement of the order of the seeing is the maximum time to avoid the trail

Population	Seeing time (minute)
NEA	$2^{-1}_{+1.8}$
MC	$2.2^{-0.8}_{+1.2}$
MB	$2.8^{-0.5}_{+0.6}$
Trojan	$6.8^{-0.6}_{+0.6}$
Centaur	90^{-77}_{+54}
KBO	150^{-50}_{+30}
Comet	$20^{-12}_{+14.2}$

Table 3.4: Table indicating the time needed for each population to move of the order of the seeing (1.5").

shape in the stack images. The times for the different population is present on table 3.4.

Chapter 4

Data reduction

In this chapter, the images calibration as well as the images photometry and astrometry performed by the pipeline are reviewed.

4.1 Calibration

Any freshly produced raw images contains all sort of instrumental bias and noises generated by the telescope optics, the CCD camera, the electronics,... These noises are sources of error when, for example, precise photometry is performed. Before any measurements and discoveries, the images must be corrected of these instrumental signatures. This is referred to as the calibration process. It comprises three main steps:

1. the bias subtraction;

2. the dark subtraction; and

3. the flat-field or flat division.

In the context of this work, the calibration steps are performed by means of scripts written with the Image Reduction and Analysis Facility[1] (IRAF), that allows to easily handle FITS images.

4.2 Bias subtraction

The bias signal is an offset signal that superimposes itself to the main signal of each pixel. It is due to the applied voltage on the CCD camera. This signal varies slightly from pixel to pixel but remains quite constant during an observation night. In order to get rid of it, we begin by recording several zero second exposure frames with the shutter closed, called bias frames. These frames contain only the bias signal (with the readout noise). Then, we combine them, generally by taking the median or the average value of the flux of each pixel, to produce a so-called master bias. This
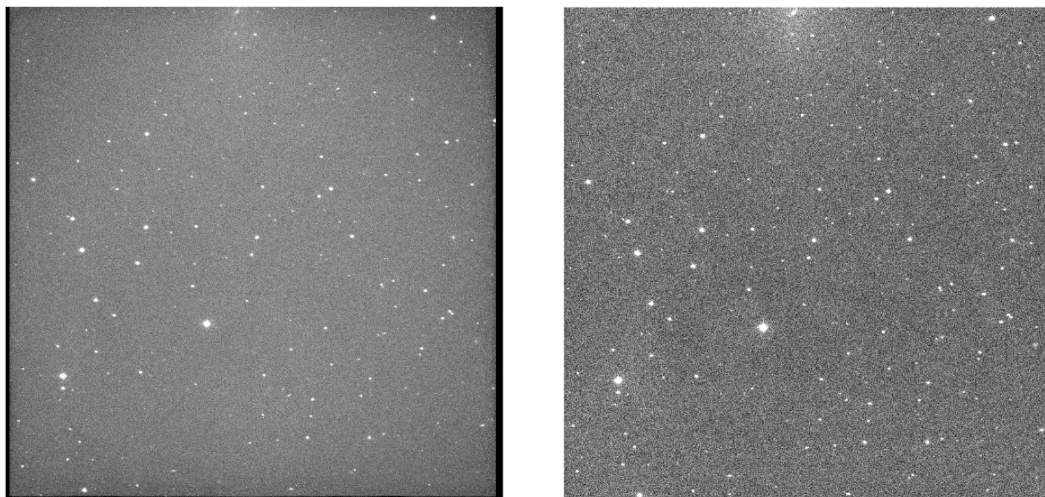
---

[1]http://ast.noao.edu/data/software

Figure 4.1: Comparison between raw (left picture) and calibrated (right picture) images.

operation reduces the readout noise[2] that unfortunately cannot be removed from the images but can be mitigated by averaging many images. The master bias is finally subtracted to the observation images. As the same offset signal is also present in dark and flat frames (see sections 4.3 and 4.4), the master bias is subtracted to these frames as well.

4.3 Dark subtraction

If the CCD temperature is not the absolute zero, some electrons, referred as thermal electrons, can cross the gap between the valence and the conduction band and create a signal, so-called the dark current, without the need of any incoming photon. Pixels accumulate thermal electrons with time. When a pixel accumulates more rapidly thermal electrons, it is referred as a hot pixel. The purpose of this step is to remove the dark current. As for the bias subtraction, a series of frames are recorded with the shutter closed but with a non zero exposure time. As far as possible, the exposure time corresponds to the one of the observation images. Here again, a master dark is created by averaging the dark frames in order to minimise the noise added to the observation images in the process. Indeed, if the number of dark frames increases, the added noise is reduced by a factor corresponding to the square root of this number of frames. The master dark is then subtracted to the observation images and to the flat frames (see section 4.4) as they are also taken with a non-zero exposure time.

4.4 Flat division

This last step is necessary because light is not recorded the same way on each pixel. This difference in sensitivity is due to the differences of sensitivity between pixels, the dust that accumulates on the camera CCD window and the vignetting of the

---

[2]The readout noise is an inherent property of any readout electronics. It corresponds to the uncertainty on the count of the charges accumulated on each pixel.

optical system[3]. These effects are corrected via the use of flat frames. These frames
are uniform sky images (without clouds) with a non-zero exposure time and usually
recorded on the twilight uniform blue sky before or after the night. All the frames
are slightly offsetted in order to remove the stars present in the field by taking the
median of all the flat frames, to form a master flat. The observation images are then
divided by the master flat. It is also worth to mention that the flat frames are filter
dependant.

4.5   Image Reduction and Analysis Facility scripts

Images are calibrated with the help of IRAF. Created in 1982 by the National
Optical Astronomy Observatories, IRAF is a system specifically designed to handle
astronomical image data (Shames and D., 1986). IRAF contains different packages of
functions that can be launched via its own interface, called the Command Language,
using its own keywords and programming language.

On the computer used to develop the `automated SSOS` pipeline, a version of
IRAF is present in the form of an environment of the Anaconda platform. There
are four main scripts that need to be launched to properly perform the calibration:
`copy2data.cl`, `datalog.cl`, `modiffilt.cl` and `prog0.cl`. The three first
scripts prepares the raw images. The `copy2data.cl` script renames the row im-
ages and transform them to FITS files. The `datalog.cl` script adds the properties
of the raw images to an annual log file. The `modiffilt.cl` script replaces the
name of several filters in the headers of the images and in the log file.

The last script, `prog0.cl`, performs the calibration strictly speaking. The
Julian date, binning and readout mode must be specified.

4.6   Photometry

The photometry is the way to retrieve the magnitude of an object from the measure-
ments of its light flux. For a given source on an image, an aperture with an adequate
size to maximize the signal-to-noise ratio, is placed around the source and the total
flux is measured inside the aperture. This flux is then normalised by dividing it by
the exposure time and background subtracted. The magnitude is then retrieved by
the following law:
$$m = -2.5 \log_{10}(F) + C,$$
where F is the flux and C is an arbitrary constant to define the origin of the scale.

In the pipeline, the photometry is automatically performed by a tool called
Source-Extractor (`SExtractor`) (Bertin and Arnouts, 1996). `SExtractor` com-
putes a background model, subtracts it to the image, retrieves the sources and
performs photometry on it, using an adaptive elliptical aperture. An illustration of
the process is given on figure 4.2.

---

[3]The vignetting occurs in an optical system when some external rays are cutted off by the edge
of a pupil in the optical path. The consequence is that the edges of the images are darker.
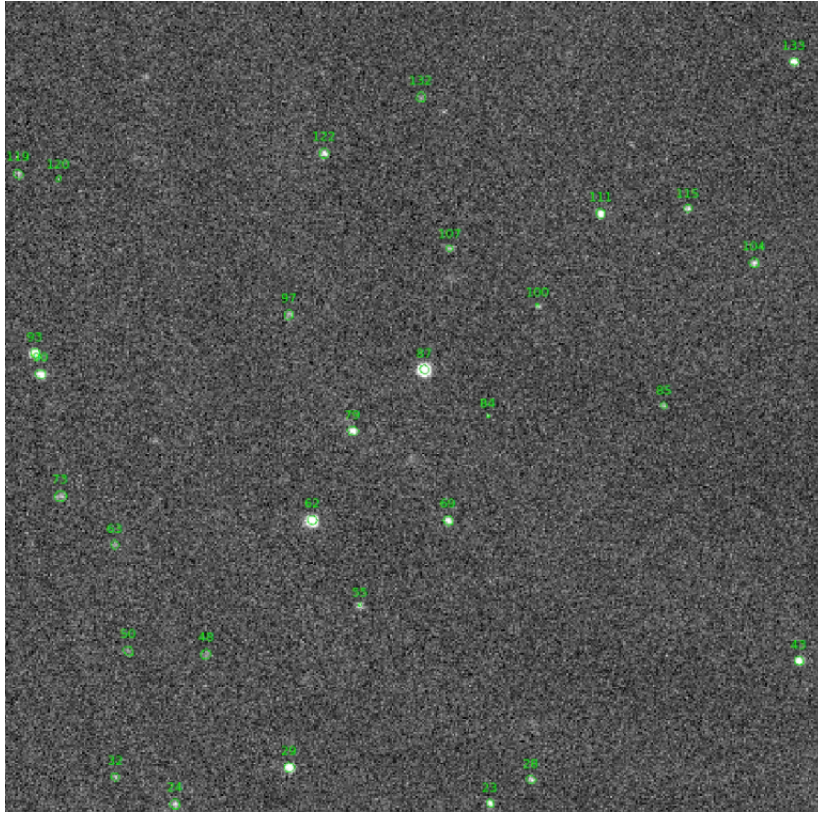
Figure 4.2: The adaptive elliptical apertures of `SExtractor`.

The magnitudes m computed by `SExtractor` are instrumental magnitudes. They do not take into account of some parameters like the light absorption by the atmosphere specific for each filter. In addition, the instrumental magnitudes are not calibrated. We can relate the apparent magnitude of an object with its instrumental magnitude by the following equation:

$$m_a = m_i + Z + \kappa \times X - A,$$

where m_a and m_i are the apparent and instrumental magnitudes, Z is the zero point, κ is the extinction coefficient, X is the airmass and A is an arbitrary constant. The zero point is computed by comparing the instrumental magnitudes of objects with apparent magnitudes from catalogue, at a given date and time. These zero point are regularly computed for the TRAPPIST telescopes and can be used to get the observational magnitude. The airmass, which is recorded in the FITS headers, is a coefficient linked to the thickness of the atmosphere crossed by the light. Its value is 1 at the zenith and increase as the altitude decreases following the law:

$$X = \frac{1}{cos(z)} \text{ with } z = 90° - altitude.$$

Differential photometry

The differential photometry is another possible photometric technique. This technique is currently not used in the pipeline. Here, we compare the target magnitude

with the magnitudes of several non-variable reference stars. These stars are chosen on the same image and close to the target. In practice, we subtract the measured target magnitude by the reference stars mean magnitude:

$$m_d = m_t - \langle m_i \rangle_{1 \leq i \leq N}. \tag{4.1}$$

Here, m_d is the differential magnitude, m_t is the target magnitude and m_i are the magnitudes of the N chosen reference stars. The subtraction operation removes all the variations of magnitude that affects both the target and the reference stars (airmass fluctuations, crossing clouds,...). In theory, one star is sufficient to remove all these effects. In practice, the possible intrinsic variation of magnitude of the star and the difference in positions between the star and the target lead to chose more than one star to improve the differential magnitude accuracy.

4.7   Astrometry

The astrometry allows to locate an object in the sky with celestial coordinates (e.g. Right Ascension (RA), Declination (DEC)). The goal is to create a one-to-one relation between the pixel and the celestial coordinates. To do so, positions of sources on an image in (x,y) are compared to their (RA,DEC) in a catalogue.

For TRAPPIST and SPECULOOS images, the astrometry is performed a first time just after the images are taken by the telescope, using the Hubble Guide Star catalogue. The observation time is precisely recorded down to 0.01 second by synchronising the telescopes with a GPS or the Liège NTP server, in order to have precise astrometric measurements. The time accuracy is especially important for fast moving objects like NEA. In the pipeline, the astrometry is performed a second time by a tool called Software for Calibrating AstroMetry and Photometry SCAMP (Bertin, 2006), using the Gaia DR2 catalogue (Prusti et al., 2016; Brown et al., 2018), from the VizieR database Ochsenbein et al. (2000), to obtain the best astrometric precision and because sometimes the astrometry on the telescope side fails.

Chapter 5

The Solar System Objects Search (`ssos`) tool

The goals of this work were to find, test and implement a pipeline to find moving targets in TRAPPIST archival data. In this chapter, we present the chosen tool dedicated to the search of moving targets. First, a description of the tool is provided. Then, various tests are described to check if this tool could be implemented and to find the best parameters for the TRAPPIST telescope.

5.1 The `ssos` tool

The `ssos` tool[1] is a recently developed program whose main goal is to search for SSOs in telescopic observations (Mahlke et al., 2019). The program is written in `python 3`. The strength of this tool lies in its remarkable capacity to adapt itself into a large variety of astronomical set-up and its numerous degrees of freedom. The main idea behind its conception was to propose a tool for smaller-scale telescope or surveys which cannot afford the complete development of such a tracking system. The `ssos` tool finds its origin in the SSO identification pipeline, used to track down SSOs in the Kilo-Degree Survey images (Mahlke et al., 2017). We discussed on several occasions with the developer, Max Mahlke, who was very interested by our experience and feedback from TRAPPIST implementation.

In order to extract all the useful information from the images, the `ssos` tool uses Source-Extractor (`SExtractor`) (Bertin and Arnouts, 1996) and the Software for Calibrating AstroMetry and Photometry (`SCAMP`) (Bertin, 2006), two packages of the astrOmatic[2] software. The complete flowchart is illustrated on figure 5.1. As an input, the path of the yet-to-process images is specified to the `ssos` tool. In a first step, the images are processed by `SExtractor`. For each image, a background model is built and subtracted to the image. All the sources containing five or more contiguous pixels and a flux higher than 1.5 sigma of the background are retrieved and properly deblended with each other. Photometry is finally performed and catalogues regrouping the pixel data are created. The parameters of `SExtractor` are contained in the `SExtractor` configuration file.

---

[1] https://ssos.readthedocs.io/en/latest/
[2] https://www.astromatic.net/
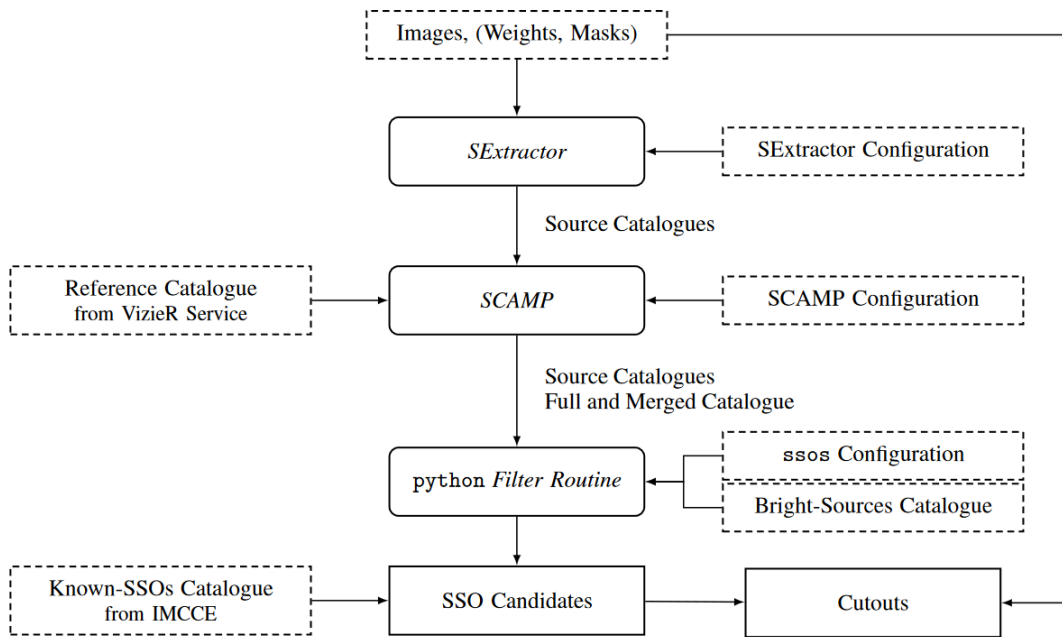
Figure 5.1: Flowchart of the ssos tool (Mahlke et al., 2019). The dashed rectangles are the inputs, the rounded-corner rectangles are the pipeline steps and the right-corner rectangles are the outputs. Some telescope and image properties such as the pixel scale, the detector gain and some keywords of the FITS header need to be indicated as inputs in the configuration files. Otherwise, the ssos tool is completely facility-independent.

In a second step, all the sources identified in all the images are linked with each other using SCAMP. The astrometry is performed and the sources from the same object in different images are associated. Again catalogues containing the astrometric positions of all the sources identified is created for each images. In addition, a catalogue regrouping all the sources of all the images are also created. An example of such a catalogue is presented on figure 5.2. This is very useful to see if ssos properly detect all the SSOs in the field.

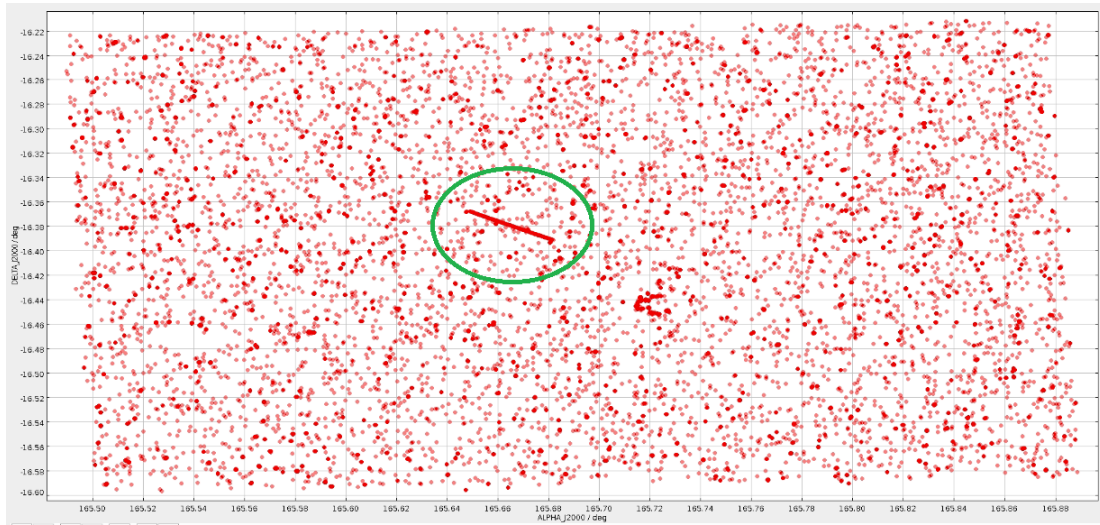Figure 5.2: An example of catalogue produced by SCAMP containing all the sources of all the images. This catalogue correspond to the night of the 06/03/20. The trail encircled in green is the path of the asteroid 1998 UO$_{19}$ in the field.

The third step separates the SSOs from the stars, galaxies and other artefacts. For this purpose, the images are ran through a set of six filters:

- number of detections;

- bad pixel;

- proper motion;

- linear motion;

- trail consistency; and

- bright-sources catalogue.

The **number of detections** filter rejects all the sources with a number of recurrences in the images lower than a certain threshold. Typically, the cosmic rays are stopped by this filter as they practically always appear on only one image.

The **bad pixel** filter goal is to remove the hot pixels. It relies on the fact that hot pixels are always the same on the pixel grid. For a given hot pixel, its positions on the grid through the images will barely change and stay around the same zone. The filter thus defines a difference limit between two positions and all the sources for which the positions difference through the images is below this limit, are excluded.

Stars and other static sources in the field begin to be removed with the **proper motion** filter. This filter has two filtering modes that can either operate separately or together. Both modes use the absolute proper motions of the sources computed by SCAMP by linearly fitting the sources coordinates over time. In the first filtering mode, the signal-to-noise ratio of the proper motion, which is the ratio between the proper motion μ and its uncertainty σ_μ, also calculated by SCAMP, is computed for each source that has not been discarded by the two previous filters: $SNR = \mu/\sigma_\mu$. The filter consists of setting a lower threshold to this signal-to-noise ratio (PM_SNR).

Sources with no proper motions like stars or galaxies exhibit a large uncertainty σ_μ resulting in a low signal-to-noise ratio. They are then more likely to be discarded by this filter. The second filtering mode involves the possibility to fix two thresholds to the proper motion itself. Each source with a proper motion below a lower threshold or above a upper threshold is discarded. This second mode gives the possibility to focus on a small range of proper motion which is often associated to a class of objects. In addition, the threshold on the signal-to-noise ratio indirectly puts a lower threshold on the proper motion, discarding all the SSOs with a proper motion value of the order of the seeing. The second mode allows a better way of searching these type of SSOs. On the other hand, the second filtering mode does not discard any artefacts with a non-linear motion.

The **linear motion** filter fits both the right ascension and the declination positions and is in a way more restrictive than the proper motion filter. The threshold is fixed on the determination parameter $R^2 = 1 - \frac{\sum_i (y_i - f_i)^2}{\sum_i (y_i - \bar{y})^2}$, with y_i the coordinate value of the data, f_i the coordinate value of the model and $\bar{y}$ the mean coordinate value. For both coordinates of each source, if the determination parameter is below the fixed threshold, the source is discarded. An optional analysis is added to this filter which computes the median absolute deviation (MAD) of a source: $MAD = median(|E_i - median(E)|)$, with E_i an observation epoch. The sources with a MAD above an upper limit are considered as outliers, but are not directly rejected.

The **trail consistency** filter looks at the morphology of the source. This filter is based on the standard deviations of the semi-major axes a and b of elliptical aperture used by `SExtractor` to perform the photometry. For each axis, the filter examine the standard deviation $std(a, b)$ through the ratio $Ratio_{a,b} = \bar{\sigma}_{a,b}/std_{a,b}$, where $\bar{\sigma}_{a,b}$ is the mean weighted uncertainties of the axes. For each source, if the ratios are below the fixed limits, the source are rejected, otherwise the source is accepted.

Finally, the last filter called **bright-sources catalogue** is more optional and tends to filter ghosts and spikes that can appear near bright objects, by setting a distance limit around these objects below which any sources are rejected. The bright objects are defined following a catalogue. It is worth to mention that the SNR threshold for the proper motion filter can depend on what we want to detect.

When all the filters have been applied, the remaining objects are called SSO candidates. The parameters of each filter can be modified in the `ssos` configuration file. The layout of this configuration file is illustrated in Appendix A and a description of the parameters is proposed below.

The `ssos` tool offers the possibility to create visual verifications of the SSO candidates. By using `SWARP` (Bertin et al., 2002), a tool that allows to resamples and co-adds FITS images, `ssos` extracts images centred on the SSO candidates (cutouts) from the observation images. By launching a specific `ssos` command, that internally use the `ArtistAnimation()` function of the `matplotlib.animation.animation` `python` module, these cutouts are shown to the user in a gif-like animation. We can then visually confirm (or not) the SSO nature of an object. Two examples of cutouts are present on figure 5.3.
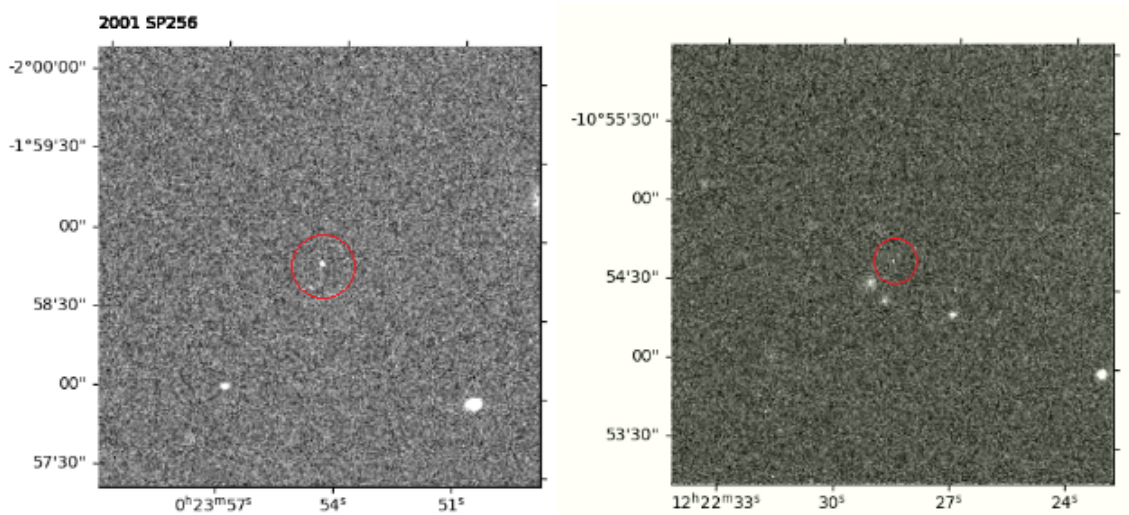
Figure 5.3: Illustrations of the identification procedure using the cutouts produced by `ssos` . The object of interest is always at the center of the images. On the left image, a real SSO (2001 SP$_{256}$) is present in the centre. On the right image, a hot pixel is present in the centre.

5.1.1 Parameters of the `ssos` configuration file and optional analysis

The layout of the `ssos` configuration file as well as examples of the parameter values is presented in Appendix A. It is divided into several parts. The first part (Image Parameters) is specific to the telescope set-up. It indicates some properties of the images and the names of the necessary header keywords. The next parts (SExtractor, Scamp, SWARP) are related to the computer itself, telling the paths of the `Sextractor`, `SCAMP` and `SWARP` files. Finally, the last part (SSO Filter Setting) is about the `ssos` parameters. In addition to the filter parameters already described in section 5.1, a series of optional analysis parameters are also present. A first series of optional parameters defines the possibility to match the SSO candidates with already-known SSOs. To do so, `ssos` use the Sky Body Tracker (SkyBoT) (Berthier et al., 2006), that identifies already-known SSOs in the field from ephemeris database (figure 5.4):

- `CROSSMATCH_SKYBOT`: activate or deactivate the choice to relate recovered SSO candidates to already-known SSOs in the field using SkyBoT.

- `CROSSMATCH_RADIUS`: the maximal distance between an SSO candidate and a already-known SSOs to be identified as one and only object.

- `OBSERVATORY_CODE`: the code of the observatory (important for SkyBoT). It contains the information of the location on Earth of the observatory (latitude, longitude and altitude).

- `FOV_DIMENSIONS`: the dimensions of the field of view in which SkyBoT identifies the already-known SSOs.
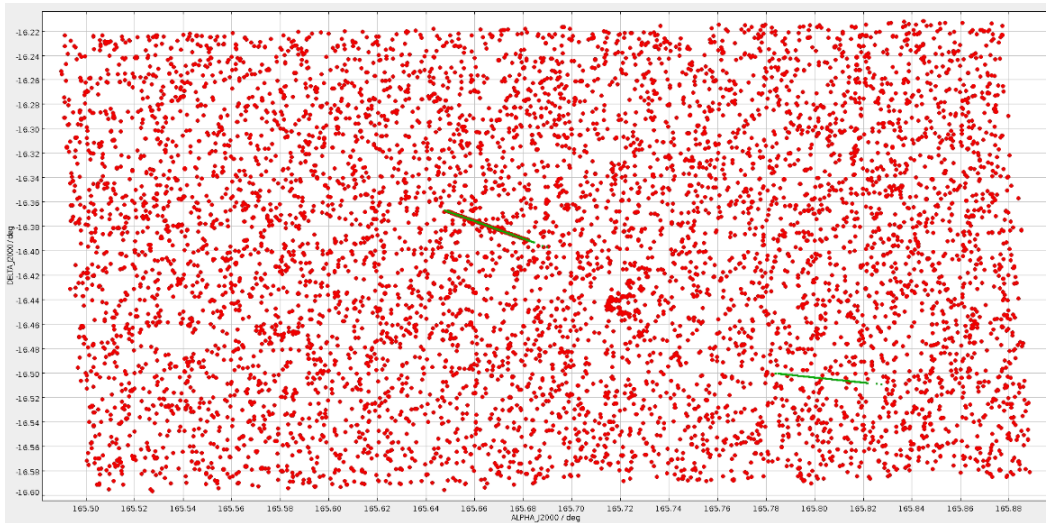
Figure 5.4: The already-known SSOs identified by SkyBoT in the field (in green), plotted on the same catalogue presented above.

The next two optional parameters are associated to the cutouts creation and size:

- EXTRACT_CUTOUTS: activate or deactivate the creation of the cutouts

- CUTOUT_SIZE: set the cutout size in pixel.

The visual verification is very useful but it can be sometimes quite hard to make the difference between an SSO and an false-positive. To reduce this difficulty, we modified the ssos code and tried to adapt the frame rate and animate the SSO candidate in the field instead of the field moving around the candidate. Reducing the frame rate improved the visual quality but it appeared that the SSO candidate is even harder to spot when it moves through the field. We then only kept the frame rate modification.

The next optional parameters concerns the photometry. The ssos tool allows to compute the SSO candidates magnitudes with a fixed aperture in a certain band filter (the filter used for the observation), always with SExtractor. It is set by two parameters:

- FIXED_APER_MAGS: activate or deactivate the fixed-aperture photometry.

- REFERENCE_FILTER: the filter used in the observations

The very last parameter, CHECKPLOTS, enhances the creation of two plots linked to the SkyBoT match.

5.1.2   The assets of **ssos**

The choice of the ssos tool as the engine for the detection of the solar system bodies is based on several arguments. First, it is written in python 3 , which is the programming language of the automated SSOS pipeline (see chapter 6).

The `ssos` tool also offers numerous degrees of freedom through different sets of parameters. Each step can be adapted to fit at the best the research for solar system bodies in the observations.

Finally, the `ssos` tool offers the desired outputs for a first attempt to create an `automated SSOS` pipeline. Notably, it offers the possibility to produce a report file for the MPC, containing astrometric and photometric measurements.

The developer, Max Mahlke, working at the Nice Observatory is happy to help and can be easily contacted.

5.2   Tests

The parameters of the `ssos` configuration file can be adjusted to improve the detection. Indeed, the `ssos` tool can also do false-positive detections and there is a possibility that some SSOs present in the field are not recovered. As illustrated by the two test studies realised by Mahlke et al. (2019), if we put lesser constraints on the parameters, it leads to the recovery of a larger number of SSOs up the the magnitude limit in the images. The drawback is that a large number of false-positive is also retrieved. At the contrary, choosing more restrictive parameters reduces the numbers of false-positive detections but also decreases the probability to recover all the real SSOs present in the images.

We tested the `ssos` tool on the same field during six different nights (19/10/2016, 20/10/2016, 21/10/2016, 25/10/2016, 28/10/2016 and 29/10/2010). The target was the ultra-cool dwarf UCDTS-90 and it was observed with TRAPPIST-South. The field was chosen for two reasons. First, we could already see some relatively bright asteroids crossing the images by eyes. Secondly, the target ecliptic latitude is only -1.97° which means aiming through the ecliptic plane where lies most of the asteroids.

As a primary requirement, the `ssos` tool has to be able to recover a maximum of already-known SSOs. Thus we checked and counted all the known asteroids present in the studied field at the mentioned dates. As a user-verification is necessary at the end of the `ssos` process, we restricted the count to only objects that can be seen by eye on the screen (the eye is a very powerful tool). The number of known SSOs for each night is given in table 5.1. All these SSOs are Main-Belt asteroids.

As a start, the `ssos` tool was launched on the images with a set of default values, registered in the TRAPPIST-South `ssos` configuration file. These values can be seen in Appendix A. The header keywords, the path to the other configuration files, the observatory code and the field of view was adapted to the telescope and computer setups. For this first trial, the trail consistency and the bright-sources catalogue filters have been disabled. According to the tests realised by Mahlke et al. (2019), while it considerably reduce the number of false-positive detections, the trail consistency also limits the number of detections of real SSOs. The results of the tests are summarised in table 5.2.

We noticed that the default value parameters already give good results concerning the already-known SSOs. The only asteroid that is not recovered by `ssos` is 2001 SP$_{256}$ during the first night (19/10/2016). Nevertheless, it is recovered during the second night (20/10/2016). Concerning the false-positive detections, the linear

Observation night	Known SSOs in the field	Name	Magnitude
19/10/2016	2	2013 YD$_{133}$	19.3
		2001 SP$_{256}$	19.6
20/10/2016	2	2000 DA$_{15}$	19.6
		2001 SP$_{256}$	19.6
21/10/2016	1	9596 P-L	18.5
25/10/2016	1	2001 YQ$_{96}$	19.5
28/10/2016	2	2000 YT$_8$	18.0
		3039 T-3	18.4
29/10/2016	2	2000 YT$_8$	18.0
		3039 T-3	18.4

Table 5.1: Number, names and apparent magnitude of already-known SSOs existing in the test observation night images and visible by eye.

Observation night	SSO candidates	Known SSOs recovered		False positive
		Recovered/total	**Name**	
19/10/2016	4	1/2	2013 YD$_{133}$	3
20/10/2016	8	2/2	2000 DA$_{15}$	
			2001 SP$_{256}$	6
21/10/2016	5	1/1	9596 P-L	4
25/10/2016	5	1/1	2001 YQ$_{96}$	4
28/10/2016	12	2/2	2000 YT$_8$	
			3039 T-3	10
29/10/2016	45	2/2	2000 YT$_8$	
			3039 T-3	43

Table 5.2: Results of the first test of the `ssos` tool on the images. For each night, the table exhibits the total amount of objects detected (SSO candidates), already-known SSOs (table 5.1) and false-positive detections recovered by `ssos`.

motion filter with a value of R_SQU_M = 0.95, considerably reduces them to just a few for the first nights. However, the two last nights seems to hold a large number of false-positive. We then focussed on the reduction of the amount of false-positive detections when we searched for the best parameter values.

An interesting parameter is DETECTIONS, associated to the number of detection filter, that sets the lower limit for the number of detections in the images. After running the `ssos` tool on the studied images, a lot of false-positive detections had only 4 or 5 detections, compared to the real SSOs that come with a much higher number of detections as we have a lot of images per night. A possible way to reduce the number of false-positive is then to increase the value of the DETECTIONS parameter. Starting from minimum 3 detections, we increased the value for each of the night to get the maximum value of the DETECTIONS parameter for which the already-known SSOs are yet recovered. The results presented in table 5.3 is the case for a minimum number of detection set to 10. This reduces a lot the number of false-positive but keep barely all the real SSOs (only one is not recovered).

The lower and upper boundaries of the proper motion filter can also be adapted to

Observation night	Known SSOs recovered	False-positive
19/10/2016	1/2	2
20/10/2016	2/2	2
21/10/2016	1/1	1
25/10/2016	0/1	0
28/10/2016	2/2	3
29/10/2016	2/2	19

Table 5.3: The `ssos` recoveries with the `DETECTIONS` set up to 10.

the velocities of the Main-Belt asteroids. Here, the `PM_LOW` and `PM_UP` parameters were respectively set to 10"/h and 80"/h. It is particularly useful to try to reduce the false-positive for the two last nights. However, it seems that it avoids the recovery of 2001 YQ$_{96}$ during the fourth night, like in the case of an increase of the `DETECTION` parameter. The results are present on table 5.4.

Observation night	Known SSOs recovered	False-positive
19/10/2016	1/2	1
20/10/2016	2/2	4
21/10/2016	1/1	3
25/10/2016	0/1	1
28/10/2016	2/2	3
29/10/2016	2/2	4

Table 5.4: The `ssos` recoveries with the `PM_LOW` and `PM_UP` parameters of the proper motion filter respectively set to 10"/h and 80"/h.

The `R_SQU_M` parameter of the linear motion filter was also investigated. A slight increase up to 0.97 also contributes to reduce the number of false-positive. The results are presents on table 5.5. However, above this value some of the asteroids are not recovered anymore.

Observation night	Known SSOs recovered	False-positive
19/10/2016	1/2	3
20/10/2016	2/2	3
21/10/2016	1/1	2
25/10/2016	1/1	3
28/10/2016	2/2	6
29/10/2016	2/2	30

Table 5.5: The `ssos` recoveries with the `R_SQU_M` parameter of the linear motion filter sets to 0.97.

We also tried to launch the `ssos` tool on the nights with the trail consistency filter on. It appeared that with a `RATIO` parameter sets to 0.15, it tends also to reduce the number of false-positive and keeps the detection of the asteroids for the first four nights. The results are present on table 5.6. However for the last two

nights, the `RATIO` parameter needs to be set to 0.01 to retrieve all the asteroids. This low value does not affect the number of false-positive.

Observation night	Known SSOs recovered	False-positive
19/10/2016	1/2	0
20/10/2016	2/2	3
21/10/2016	1/1	2
25/10/2016	1/1	3

Table 5.6: The results of the first four nights with the trail consistency filter activated and a `RATIO` parameter sets to 0.15.

Finally, we ran a test on the nights with the bad pixel filter off to see if a lot of hot pixels were present in the images. The results are the same as with the bad pixel filter on. Either there is nearly no hot pixel on the images or they are removed during previous steps.

Conclusion of the tests

We focused here mainly on the reduction of false-positive detections. The number of detections and the proper motion plays an important role as they strongly reduce the number of false-positive nearly without reducing the efficiency of `ssos` . As a consequence, we fixed the minimum number of detections to 10 as a start. The linear motion filter can be slightly increased but it needs to be handled with care as a too high value of its parameter can drop the number of real SSOs recovered. We choose to keep the value of 0.95. The trail consistency filter is evaluated as too strong and for now is not being used in the pipeline.

It is worth to mention that the values of the parameters strongly depend on what kind of object we want to detect, especially regarding the apparent velocity of the objects. We can illustrate this with an example involving the NEOs and the Kuiper belt objects. The NEOs are moving very fast and do not stay long in the images. As a consequence, the value of the `DETECTIONS` parameter of the number of detections filter must not be too high otherwise these objects will not be recovered by the `ssos` tool. In return, we can set high values for the `PM_SNR` or the `PM_low` parameters of the proper motion filter. At the contrary, far objects from the Kuiper belt require a very low value of the `PM_SNR` parameter to be detected but the `DETECTIONS` parameter can be quite high as they slowly move with time through the images and there are many more images with them recorded than fast Near-Earth Asteroids that leave the field of view more rapidly.

This multiplicity of the parameters is not inconsistent with the creation of an automated task program. Indeed, we can run the `ssos` tool several times on the same set of images with different sets of parameter values adapted for the population we are targeting. It will of course take more computational time.

Chapter 6

The automated SSOS pipeline

After testing and validating the `ssos` tool on TRAPPIST data, the other main task of this work was to link it to the TRAPPIST dataflow to automatically find and retrieve the informations (astrometry and photometry) from the TRAPPIST images after each night. For that, a program, that we call the `automated SSOS` pipeline, was implemented. It is described in detail in this chapter. The pipeline includes notably the image calibration scripts and the `ssos` tool. Its main outputs are the lightcurves and the astrometric and photometric measurements of the detected SSOs.

6.1 Pipeline overview

The pipeline was developed in `python 3` [1]. This programming language is particularly useful regarding its large amount of available modules, guaranteeing a large freedom and allowing us to deal with the computer system.

The `automated SSOS` pipeline is installed on a computer on which new observation nights are uploaded everyday around noon. The pipeline works either in a passive or active way. In passive way, the pipeline is automatically launched on observations from the previous night and freshly transferred to the computer.

The active way allows an external user to manually launch the pipeline on one or several observation nights. It is particularly useful if we want to search for SSOs in the telescope databases. We only has to upload the data from the selected nights on the computer and ask the pipeline to process all the available observation nights. It is also useful to perform some tests or to start again the pipeline on a specific night if an error has occurred before.

The complete flowchart of the `automated SSOS` pipeline is represented on the figure 6.1. The only input of the pipeline are the images, uploaded on the computer in a compressed format. For a given observation night to process, the `automated SSOS` pipeline follows five main steps:

1. **Pre-processing**: raw images are uncompressed and copied in a specific directory waiting to be calibrated.

---

[1] https://www.python.org/

2. **Pre-sort**: in this folder, raw frames are sorted and organised into sub-folders according to their binning and readout mode.
3. **Calibration**: for each sub-folder, the frames are calibrated and stored in a second directory.
4. **Post-sort**: freshly calibrated frames are once again sorted following the name of the target.
5. **SSOs search**: for each target, calibrated images are processed with the `ssos` tool in order to find potential SSOs. A MPC report is produced and it is sent to the MPC. In addition, the lightcurves of the SSO candidates are built from the photometric measurements and detection statistics are computed.

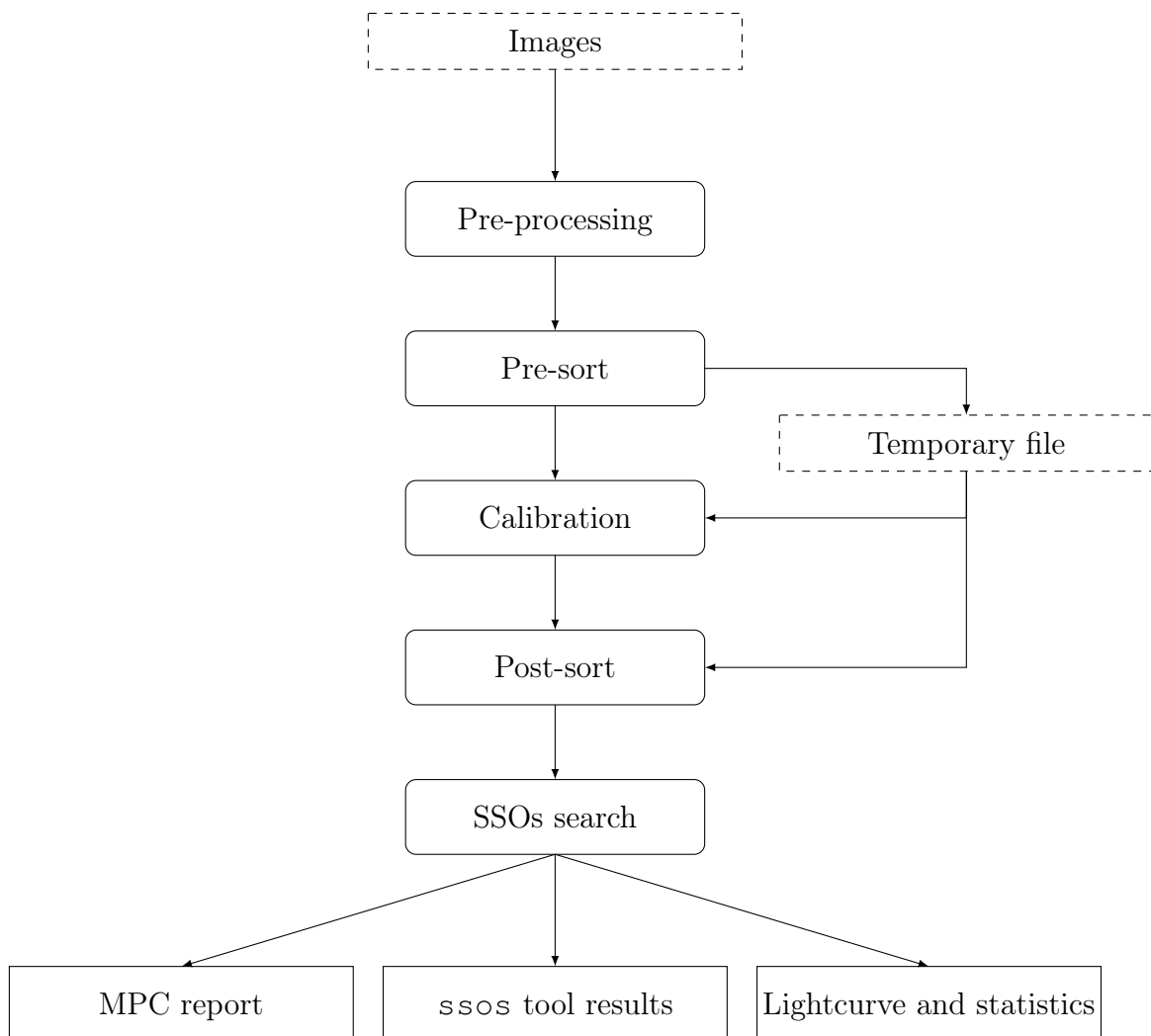Figure 6.1: Flowchart of the `automated SSOS` pipeline. The dashed rectangles are the inputs, the rounded-corner rectangles are the pipeline steps and the right-corner rectangles are the outputs.

Basic logging is also performed in order to keep track of each step of the pipeline. It is particularly useful to monitor the processing of a large number of observation nights. If an error occurred, it is recorded into the log file.
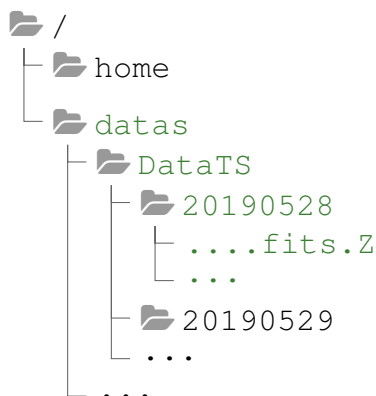
6.2 The flowchart

Here, we describes the inputs, outputs and each step of the `automated SSOS` pipeline as well as the `python` modules and functions used to build the pipeline. In addition, it makes the link with the computer by indicating the directories names involved in the process.

As an example, we assume here that we want to process the observation of the 28/05/2019 night carried out by TRAPPIST-South. All the examples and path trees will be illustrated with this observation date.

6.2.1 Inputs

The only inputs are the raw images (or frames) from the observation night we want to process. They are stored in an auxiliary hard drive called `datas` and organised following the name of the telescope and the date of observation. Each raw image appears in the form of a UNIX-compressed file (`.Z` file). The name of the folder containing the raw images of one night is the date of the observation, parametrised in the form YYYYMMDD (e.g. 20190528). The path is highlighted in green on the following path tree:

```
📂 /
├── 📂 home
└── 📂 datas
    ├── 📂 DataTS
    │   ├── 📂 20190528
    │   │   ├── ....fits.Z
    │   │   └── ...
    │   ├── 📂 20190529
    │   └── ...
    └── ...
```

Here, `DataTS` is the TRAPPIST-South directory.

New nights are daily uploaded on the computer, where they will be automatically stored in the right telescope directory and with a properly parametrised name.

6.2.2 Pre-processing

This first step is purely practical and helps to prepare the images for the calibration. The raw images of the chosen night is first copied from the `datas` drive to the `home` drive in the directory attached to the corresponding telescope, and stored in a date labelled folder. For TRAPPIST-South, the directory path is `/home/user/TRAPPIST/trappistraw`. This directory represent the input directory for the calibration and is rooted as the following:

```
📂 /
├─ 📂 home
│  └─ 📂 user
│     └─ 📂 TRAPPIST
│        └─ 📂 trappistraw
│           └─ 📂 20190528
│              ├─ ....fits
│              └─ ...
│        └─ ...
│     └─ ...
│  └─ ...
└─ 📂 datas
```
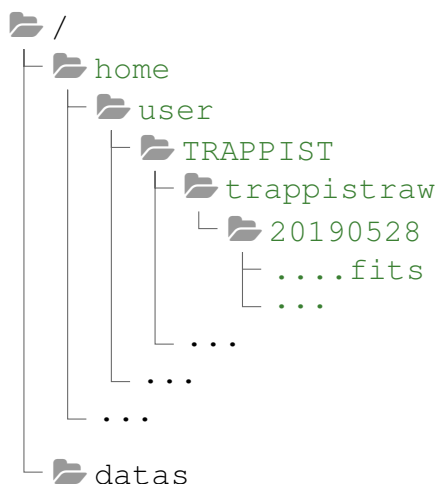
After that, each image is uncompressed with the `uncompress` shell command.

For now, when the `automated SSOS` pipeline is ran on a specified night, the date must be entered in the form YYYYMMDD on the command prompts. All other form will raise a `ValueError` exception. If there is no new observations on the desired date, the pipeline raise a `FileNotFoundError` exception. Before the images are copied into the `home` drive, the pipeline check if there is sufficient space on the disk to store the images. Otherwise, a `MemoryError` exception is raised.
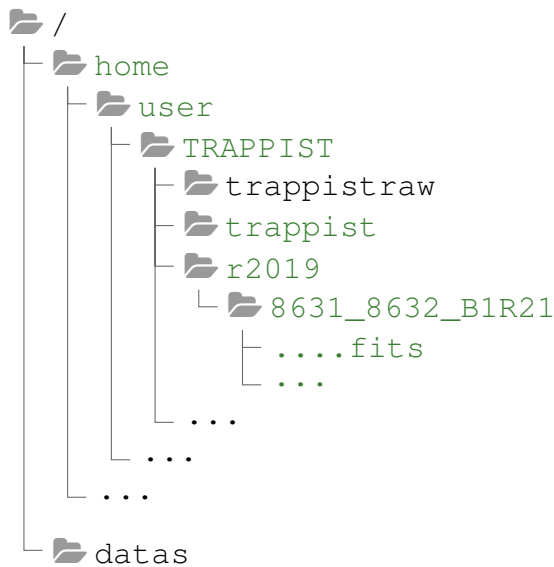
6.2.3   Pre-sort

The raw images are then sorted a first time following their binning and readout mode, as these two parameter values are essential for the calibration. Subfolders are created for a given binning and readout mode with a name of the form: TRAP_α_1_α_2_Bα_3Rα_4, with α_1, α_2, α_3, α_4 some numbers. The α_1 number represents the last 4 digits of the integer part of the observation Julian day. Then α_2 is $\alpha_1 + 1$, α_3 is the binning (1 or 2) and α_4 is the readout mode (1 or 2). The dark, bias and flat frames are also kept into two sub-folders called Calibration and AutoFlat.

The information relative to the Julian day, the binning and readout mode is retrieved from the image header using the file handling function from the `astropy.io.fits` module.

6.2.4   Calibration

For a given binning and readout mode, raw images are calibrated using the IRAF scripts described in chapter 4. After many tests, we managed to incorporate these scripts in the `automated SSOS` pipeline.

The calibrated images and the master bias, dark and flat frames are stored into a folder with a name almost identical to the one used during the pre-sort step, in a directory depending of the telescope and the year of observation. For our example, this directory is represented in green in the following path tree:

```
📁 /
├── 📁 home
│   └── 📁 user
│       └── 📁 TRAPPIST
│           ├── 📁 trappistraw
│           ├── 📁 trappist
│           ├── 📁 r2019
│           │   └── 📁 8631_8632_B1R21
│           │       ├── ....fits
│           │       └── ...
│           └── ...
│       └── ...
│   └── ...
└── 📁 datas
```

As several science targets (then several fields) can be observed during a single night, the pipeline can have several folders with different binning and/or readout mode to process. In that case, the folders are processed separately. Sometimes, the corrects master bias, dark or flat frames are not available for one of these folders and the calibration fails. When that occurs, an error message is written in the log file but the process is not interrupted. Simply, the information written in the temporary file about the concerned folder are removed. It avoids to launch the `ssos` tool on images that are not properly calibrated.

6.2.5 Post-Sort

As the `ssos` tool works for a given field, the newly calibrated images are sorted a second time following the target name.

To multiply our ways of detection, we also add the possibility to stack the images. In this way, fainter objects can be found and tracked down by the `ssos` tool. Typically, for any observation with an exposure time lower than 30 seconds, images are stacked to improve the SNR and detection limit. The number images to be stacked depends on the apparent velocities of the observed SSOs (see chapter 3). For that, we use the `pp_combine` and `pp_prepare` python modules, as part of the `photometry pipeline` package (Mommert, 2017) also based on SExtractor and SCAMP.

6.2.6 SSOs search

The launch of the `ssos` tool requires that WCS information - used to assign RA and DEC coordinates to sources on the sky - must be present in the header of the FITS images. Usually, it is the case for the TRAPPIST telescopes. However, it appeared that often a few images inside a single night miss the WCS. It happens for about 4/100 images in average. As a consequence, it was decided to filter and remove these images, instead of computing the WCS for each of them, as usually

these images are anyway useless (affected by clouds, bad centring,...). The small number of bad images does not impact the result of the `ssos` tool.

The lightcurves of each retrieved SSO candidates are built from each `ssos` tables. They are done by using the `matplotlib.pyplot` module. In addition to that, some statistics including the percentages of already-known small bodies recovered by the `ssos` tool are computed.

6.2.7   Outputs

At the end of the procedure, the `automated SSOS` pipeline launches the `ssos` command that opens the cutouts, previously computed by `ssos` . The pipeline waits for the intervention of an external user to sort the real SSOs from false detections. The lightcurves of the false-positive are deleted. Finally, a MPC report is computed, containing all the useful information related to the observation of the detected SSOs. An example of such a report is present on figure 6.2.

```
COD I40
CON E. Jehin, STAR institute
CON ejehin@uliege.be
MEA G. Sicorello
TEL 0.60-m reflector + CCD
COM TRAPPIST-South
NET Gaia-DR2

00027        C2020 01 23.18890812 09 05.94 +01 16 51.1                    I40
00027        C2020 01 23.18941212 09 05.93 +01 16 51.0                    I40
00027        C2020 01 23.18992012 09 05.94 +01 16 50.9                    I40
00027        C2020 01 23.19041312 09 05.96 +01 16 51.2                    I40
00027        C2020 01 23.19090512 09 05.96 +01 16 51.0                    I40

                          ...
```

Figure 6.2: An example of MPC report. Only the first lines are shown, concerning the asteroid (27) Euterpe. An MPC report can contain information about more than one small body. Here, the different columns correspond to the SSO name, the date of observation, the positions (RA, DEC) and the observatory code.

6.3   How to run the pipeline

The `automated SSOS` pipeline can be started from anywhere in the command prompt. At present, the pipeline must be called from its main file, a shell file called `./start.sh` . If we want to launch the pipeline on a specific night and telescope, we enter the following command in the command prompts:

```
$ ./start.sh  <telescope_id> <observation_night>
```

The command line argument `<telescope_id>` tells the pipeline in which telescope folder it needs to collect the data. The table 6.1 shows the identifier for each telescope. For now, the pipeline only processed TRAPPIST-South data, but it is ready to work on other telescopes data. The only parameters that change are some header keywords and the telescope properties (location, plate scale,...). The command line argument `<observation_night>` represents the name of the night

folder in the YYYYMMDD form. As a reminder, the observation corresponding to a certain date begins on the evening of the date and end of on the morning of the day after. As an example, the observation of the 28/05/2019 occurs between the 28/05/2019 and the 29/05/2019 and must be written in the form 20190528 in the command prompt.

TRAPPIST	Identifier	SPECULOOS	Identifier
TRAPPIST-South	ts	SPECULOOS-South 1	sso1
TRAPPIST-North	tn	SPECULOOS-South 2	sso2
		SPECULOOS-South 3	sso3
		SPECULOOS-South 4	sso4
		SPECULOOS-North 1	sno1

Table 6.1: The telescope identifiers for the `automated SSOS` pipeline.

If we want to process several nights in one run, we can write the dates successively:

```
$ ./start.sh  <telescope_id> <night1> <night2> ...
```

As the dark, bias and flat-field files can be reused to calibrate several nights (their validity is about one week), the pipeline processes the observations one at a time.

Finally, to launch the `automated SSOS` pipeline on all the nights of a telescope folder, we use the argument `all`:

```
$ ./start.sh  <telescope_id> all
```

6.4   Encountered problem

The major problem was to integrate the calibration process. The IRAF scripts for performing the calibration works very well by their own when they are manually called in the right environment. Nevertheless, many problems appeared when we tried to launch them from a `python` script.

There were two major issues. The first one was that it is needed to work inside the IRAF environment of the Anaconda system, in order to launch the calibration. That cannot be set from a python script. The second one was that the IRAF script cannot be properly launched from a `python` script.

To be enable to go in and out the IRAF environment, we use a shell script as the main file of the `automated SSOS` pipeline. From it, it was possible to launch `python` scripts inside or outside of any Anaconda environment. In the shell script, using the commands `source` and `conda` commands, we were enable to enter and exit the environment:

```
source /home/user/miniconda3/bin/activate iraf37
python /home/user/Softwares/IRAF/scriptsTS/irafLauncher.py
conda deactivate
```

Overcoming the second problem was more tricky. We needed to use the `PyRAF` python module. `PyRAF` is as very useful tool to deal with the IRAF keywords and programming language. Notably, we can use these inside a python script. Even better, one is enable to build IRAF-like program that can be ran from IRAF. We used a `PyRAF` method that translates an IRAF script into a `python` function. We needed first to define the IRAF script path as an IRAF task, using the `iraf.task()` function of `PyRAF`. Then, we invoked the `getcode()` method on our newly defined task to obtain a `python` function equivalent to the IRAF script. We finally integrated these functions in a `python` script and used it for the calibration.

6.5   Results

6.5.1   Computational time

The time needed to run the `automated SSOS` pipeline was estimated for 9 nights between the 21/02/2020 and the 23/03/2020. In average, the pipeline takes about 26.95 minutes to process a night. However, the needed time greatly depends on the number of images and can vary between 20 minutes and 40 minutes, as we see on the figure 6.3 on which was plotted the time in function of the number of images per night. Here, we did not count the nights for which one of the calibrations encountered an error due to a lack of master files. For these nights, the required computed time was skewed as it was reduced by the calibration error. In any case, as the `automated SSOS` pipeline is expected to work after each night, the required time does not pose any problem regarding its execution.
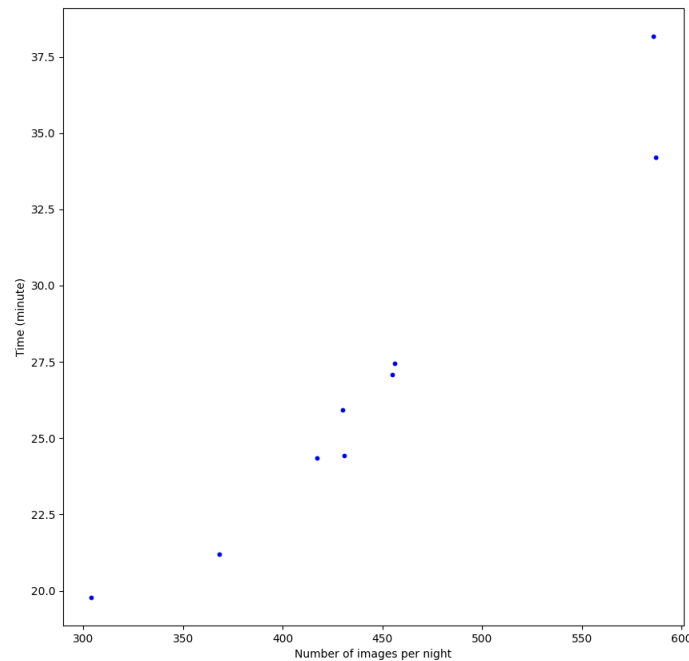

Figure 6.3: Required time on the used computer (processor: Intel Core i7-7800X CPU @ 3.50GHz x 12; RAM: 64 Gb) to run the pipeline in function of the number of images for a night.

6.5.2   Lightcurves

The SSO candidate lightcurves is the most useful end of product of the pipeline to perform some science analysis. The lightcurves are mainly used to characterize the small bodies rotation period, as explained in chapter 1. We present here preliminary lightcurves computed on one or several nights.

On figure 6.4, we show the lightcurve of the asteroid (3395) Jitka, taken on the night of the 22/01/2020.
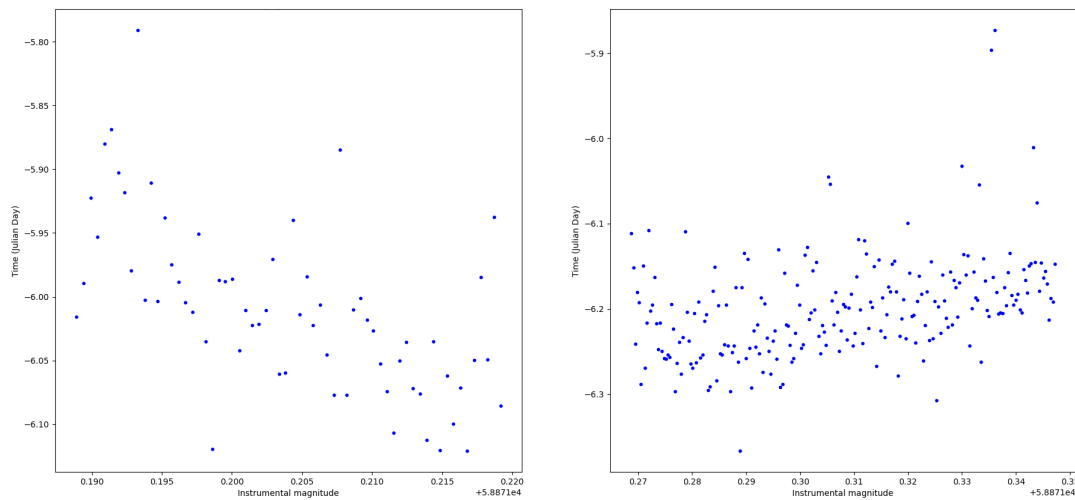

Figure 6.4: Lightcurves of (3395) Jitka, retrieved during the night of the 22/01/2020.

We have also retrieved the lightcurves of asteroids recovered during several nights. They are represented on figures 6.5, 6.6 and 6.7. The asteroids (324) Bamberga and (208) Lacrimosa were the science targets. The asteroid (3249) Musashino was present in the observed field too.
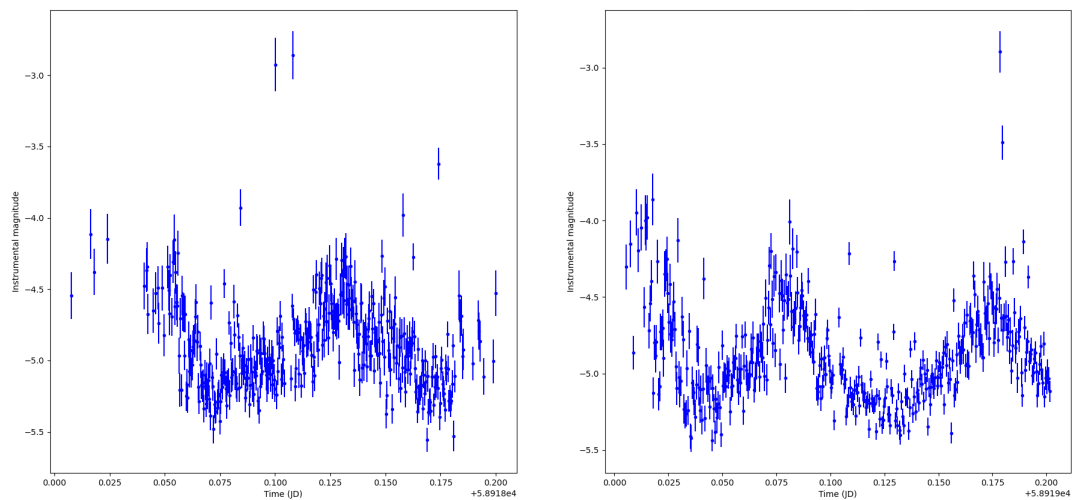
Figure 6.5: The asteroid (3249) Musashino retrieved during two nights: 09/03/2020 (left), 10/03/2020 (right). Its rotation period of 4,5 hours.
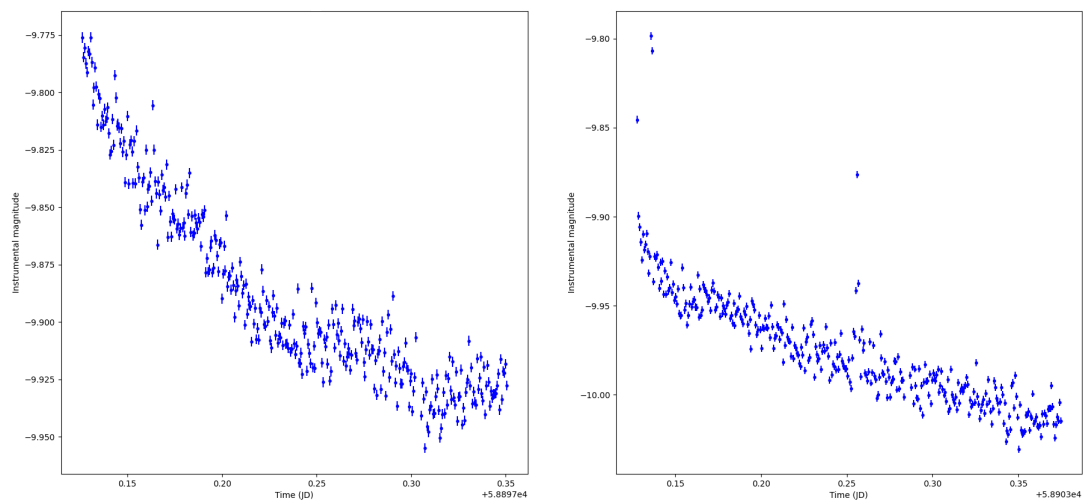

Figure 6.6: The (324) Bamberga lightcurve during two nights: 17/02/2020 (left), 23/02/2020 (right). Bamberga is a slow rotator (29,1 hours).
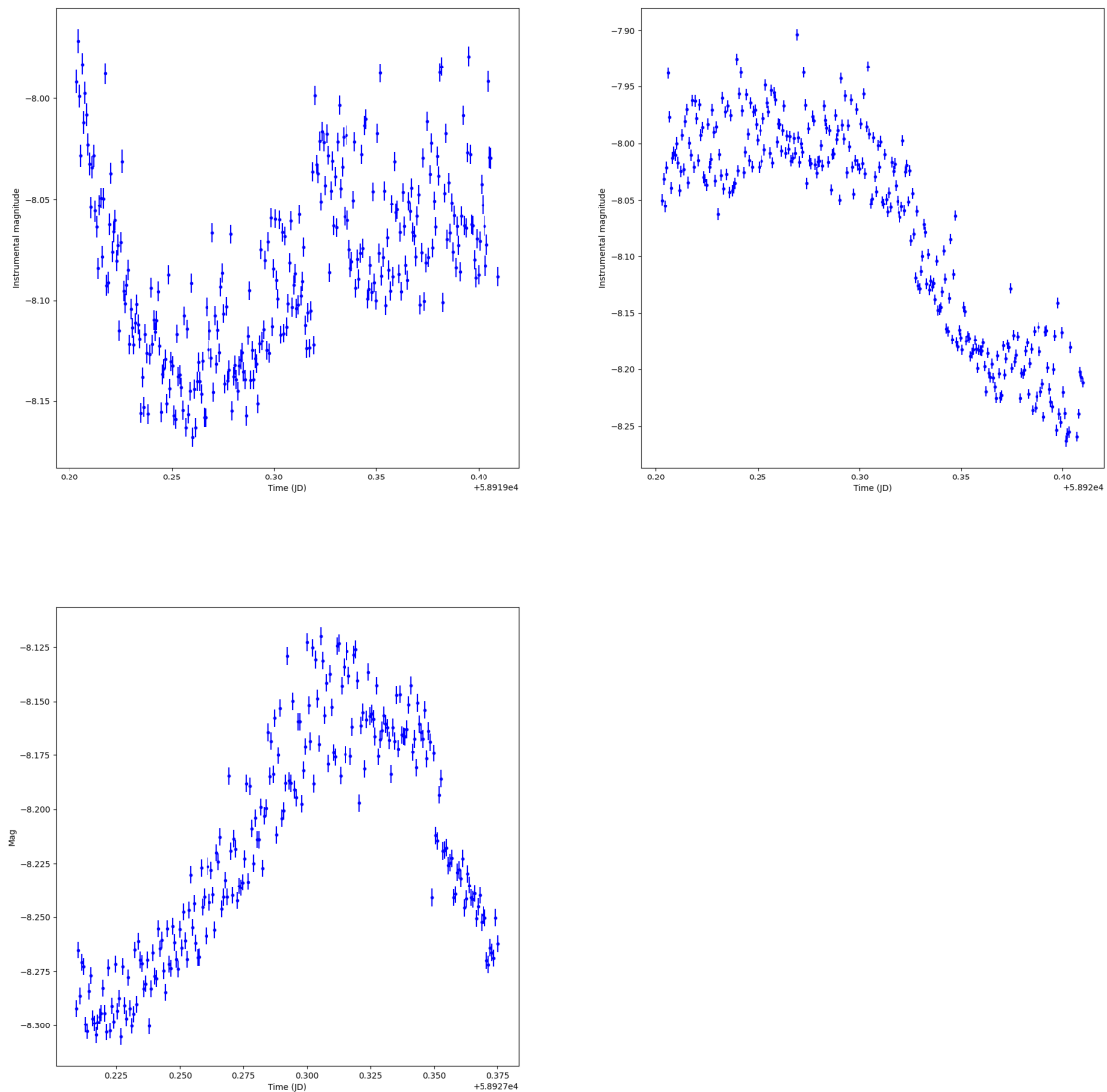
Figure 6.7: The asteroid (208) Lacrimosa retrieved during three nights: 09/03/2020 (first lightcurve), 11/03/2020 (second lightcurve) and 18/03/2020 (third lightcurve). It has a rotation period of 14.1 hours

6.5.3   Detection statistics

This section is about the ability of the `ssos` tool to recover the already-known SSOs of different magnitude. As a test, the `automated SSOS` pipeline was ran on 58 nights between the 20/01/2020 and the 23/03/2020 (last night before TRAPPIST-South telescope operation had to be stopped because of the Covid-19 crisis). A total of 22 asteroids was detected between magnitude 16.5 and 20.5. The results are summarized in the two histograms presented in figure 6.8. The first histogram shows the number of detections in function of the magnitude and the second histogram illustrates the percentage of SSO recoveries in function of the magnitude. The

small bodies and their apparent magnitudes were obtained from the SkyBoT service, implemented in the `ssos` tool. In both diagrams, the gap between 17.5 and 17.9 is because no SSOs was present at these magnitudes in the studied fields. The data from which these histograms are plotted are present on table 6.2.

Magnitude	Recovered	Total
16.5 - 16.9	1	1
17 - 17.4	2	3
18 - 18.4	4	5
18.5 - 18.9	3	4
19 - 19.4	4	6
19.5 - 19.9	7	17
20 - 20.4	1	23

Table 6.2: Table showing the recovery rate of the SSO pipeline for the tests performed with TRAPPIST-South. The second column displays the number of asteroids recovered per magnitude interval. The third column gives the total number of SSOs present in the observed fields (identified with SkyBoT). There was no SSOs with a magnitude below 16.5 or between 17 - 17.4.
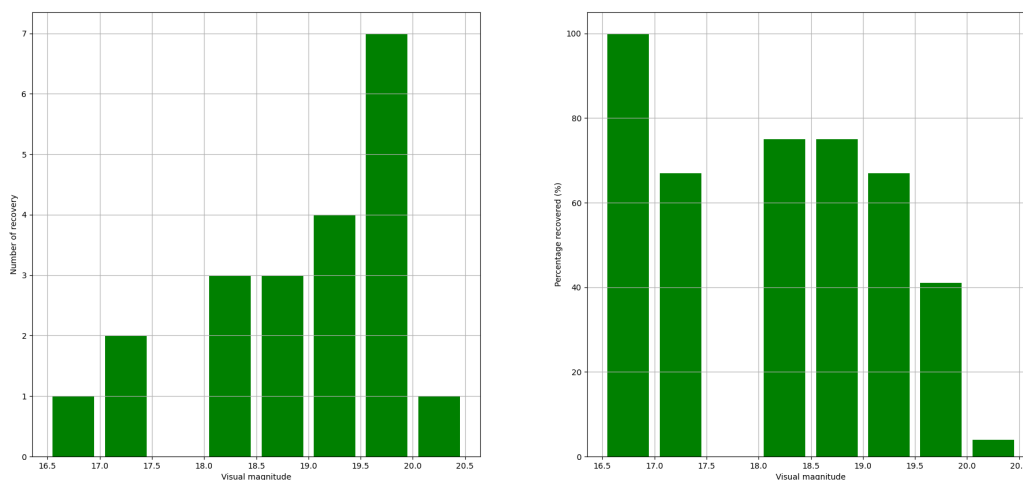
Figure 6.8: Number (left figure) and percentage (right figure) of already-known asteroids detected in function of the magnitude. Asteroids are grouped by 0.5 magnitude intervals (16.5 - 16.9, 17 - 17.4,...)

This detection rate is directly related to the chosen parameter values in the previous chapter. As we can see, the detection works pretty well up to a magnitude of 19, with a high recovery rate of more than 75% in average. Note that the statistics are not very large for the intervals up to mag 19. Then, the detection quality rapidly drops because the asteroids are too weak and the SNR is too low to detect them.

About 40% are still detected between 19 and 19,5 while nearly none are recovered for magnitude larger than 20. This corresponds well to the magnitude limit of TRAPPIST.

Chapter 7

General conclusion and perspective

The several telescopes of the TRAPPIST and SPECULOOS networks take hundreds of images of only 1 to 3 fields per night usually, totalizing hundreds of images from 10 s to 60 s typically on each of these fields. Considering the fields of view of these telescopes, images of hundreds of celestial objects are captured in these images and among them, moving objects like asteroids and comets. Until now, these images were mostly used to study the main target of the planned observation but they contain hundreds of small solar system objects to be measured.

In this work, we have described a new program, called the `automated SSOS` pipeline, whose primary goal is to detect moving targets captured in the TRAPPIST or SPECULOOS images, identify them, measure their positions and magnitudes. Thanks to a set of parameters, allowing to define an apparent velocity range and the number of detections in the images, the `ssos` search tool it can be adapted to detect a maximum of objects of different small body classes. When detected, the lightcurves of these objects are computed and give useful information. Through the lightcurve, the rotation period and 3D shape can be determined in the case of an asteroid. Photometric and astrometric measurements are compiled in formatted reports and sent to the MPC. These reports contribute to refine the orbital parameters of the small bodies. It is particularly important in the case of NEOs to predict well in advance a collision with the Earth.

As the pipeline works also on fresh data, it will be possible also to discover a new comet or asteroids. Especially, for TRAPPIST and SPECULOOS surveys programs, the telescopes do not always aim near the ecliptic plane and objects on highly inclined orbits can be found.

Perspectives

There are still several things to improve.

It would better to run the pipeline as soon as the night is finished and locally in the observatory to not wait for the new calibrations (previous night calibrations are usually good) and for the data to be transferred to Liège. This might be crucial to be the first to find a new object.

We should also use the `photometry pipeline` (Mommert, 2017), a `python` software package, to perform really good photometry. For the detection of object

to be reported to the MPC and for raw lightcurves the first methode is enough and fast. To obtain the most precise lightcurves it will be needed to implement the differential photometry. First testing have been very encouraging and would provide light curves with a much better precision.

Photometric measurements could also allow the study of known or even new variables stars with very long lightcurves. TRAPPIST and SPECULOOS datasets should be very useful for that as the telecopes can stay on one field for up to 10 to 20 nights and produce very detailed long lightcurve of variable stars.

A track and stack strategy to combine the images, depending on the kind of object to detect, would allow to increase the limiting magnitude and find more objects. This is especially true for the faint and distant TNOs.

We have only reduced and analysed 3 months of TRAPPIST-South data while there are 10 years in the archive to be processed, 4 years of TRAPPIST-North data and two years of the SPECULOOS south telescopes totalizing millions of images.

Appendix A

Configuration files of the **ssos** tool

`TS_setup.ssos`

```
# TRAPPIST South configuration file for the ssos tool

# ------
# Image Parameters

SCI_EXTENSION           0                       # Science Extension of FITS file
FIX_HEADER              False                   # Adjust/remove bad distortion parameters inplace
WEIGHT_IMAGES           False                   # Absolute path to weight images for SExtractor run
RA                      CRVAL1                  # Header keyword of right ascension in degree
DEC                     CRVAL2                  # Header keyword of declination in degree
OBJECT                  OBJECT                  # Header OBJECT keyword
DATE-OBS                DATE-OBS                # Header keyword for start of observation in ISOT
                                                  or MJD format
FILTER                  FILTER                  # Header keyword for observation filter/band
EXPTIME                 EXPTIME                 # Header keyword for exposure time

# ------
# SExtractor

SEX_CONFIG              $HOME/miniconda3/lib/python3.7/site-packages/ssos/semp/ssos.sex
# Path to SExtractor config file
SEX_PARAMS              $HOME/miniconda3/lib/python3.7/site-packages/ssos/semp/ssos.param
# Path to SExtractor param list
SEX_FILTER              $HOME/miniconda3/lib/python3.7/site-packages/ssos/semp/gauss_2.5_5x5.conv
# Path to SExtractor filter file
SEX_NNW                 $HOME/miniconda3/lib/python3.7/site-packages/ssos/semp/default.nnw
# Path to SExtractor neural network file

# ------
# SCAMP

SCAMP_CONFIG            $HOME/miniconda3/lib/python3.7/site-packages/ssos/semp/ssos.scamp
# Path to SCAMP config file
REMOVE_REF_SOURCES      False
# Remove reference sources before pattern matching

# ------
# SWARP

SWARP_CONFIG            $HOME/miniconda3/lib/python3.7/site-packages/ssos/semp/ssos.swarp
# Path to SWARP config file

# ------
# SSO Filter Settings

FILTER_DETEC            True                    # Filter by number of detections
DETECTIONS              1,2,3                   # Number of detections to filter
```

```
FILTER_PM               True                        # Filter by proper motion range
PM_LOW                  0                           # Lower proper motion limit / "/h
PM_UP                   300                         # Upper proper motion limit / "/h
PM_SNR                  0.5                         # Lower limit of proper motion SNR

FILTER_PIXEL            True                        # Filter by pixel margin
DELTA_PIXEL             2                           # Lower limit of pixel margin

FILTER_MOTION           True                        # Filter by linear motion
IDENTIFY_OUTLIER        False                       # Flag outlier and fit subgroups
OUTLIER_THRESHOLD       2                           # Threshold in DeltaEpoch / MAD
R_SQU_M                 0.95                        # Minimum goodness-of-fit

FILTER_TRAIL            False                       # Filter by constant trail size
RATIO                   0.25                        # Minimum ratio of mean/outlier

FILTER_BRIGHT_SOURCES   False                       # Filter by distance to bright source
BRIGHT_SOURCES_CAT      REFCAT                      # REFCAT or Path to local catalog
DISTANCE                300                         # Minimum distance to source in "
MAG_LIMITS              -99,99                      # Magnitude limits applied to bright sources
                                                      catalogue


# ------
# Optional Analyses

CROSSMATCH_SKYBOT       True                        # Cross-match sources with SkyBoT
CROSSMATCH_RADIUS       10                          # Upper distance in " to count as match
OBSERVATORY_CODE        I40                         # IAU Observatory code for SkyBoT query
FOV_DIMENSIONS          0x0                         # Edge lengths of query region / deg,
                                                      0x0 - automatically

EXTRACT_CUTOUTS         True                        # Save cutouts of source detections
CUTOUT_SIZE             256                         # Cutout size in pixel

FIXED_APER_MAGS         False                       # Compute fixed aperture magnitudes for color
                                                      indices
REFERENCE_FILTER        I+z                         # Detection filter in dual-img mode

CHECKPLOTS              SKYBOT_RESIDUALS,SKYBOT_PM  # Checkplots to generate. Put False for
                                                      no checkplots
```

Bibliography

J. Berthier, F. Vachier, W. Thuillot, P. Fernique, F. Ochsenbein, F. Genova, V. Lainey, and J.-E. Arlot. Skybot, a new vo service to identify solar system objects. 351:367, 06 2006.

E. Bertin. Automatic Astrometric and Photometric Calibration with SCAMP. In C. Gabriel, C. Arviset, D. Ponz, and S. Enrique, editors, *Astronomical Data Analysis Software and Systems XV*, volume 351 of *Astronomical Society of the Pacific Conference Series*, page 112, July 2006.

E. Bertin and S. Arnouts. SExtractor: Software for source extraction. *aaps*, 117: 393–404, June 1996. doi: 10.1051/aas:1996164.

E. Bertin, Y. Mellier, M. Radovich, G. Missonnier, P. Didelon, and B. Morin. The TERAPIX Pipeline. In David A. Bohlender, Daniel Durand, and Thomas H. Handley, editors, *Astronomical Data Analysis Software and Systems XI*, volume 281 of *Astronomical Society of the Pacific Conference Series*, page 228, January 2002.

F. Braga-Ribas, B. Sicardy, J. L. Ortiz, C. Snodgrass, F. Roques, R. Vieira-Martins, J. I. B. Camargo, M. Assafin, R. Duffard, E. Jehin, and et al. A ring system detected around the centaur (10199) chariklo. *Nature*, 508(7494):72–75, Mar 2014. ISSN 1476-4687. doi: 10.1038/nature13155. URL http://dx.doi.org/10.1038/nature13155.

A. G. A. Brown, A. Vallenari, T. Prusti, J. H. J. de Bruijne, C. Babusiaux, C. A. L. Bailer-Jones, M. Biermann, D. W. Evans, L. Eyer, and et al. Gaia data release 2. *Astronomy and Astrophysics*, 616:A1, Aug 2018. doi: 10.1051/0004-6361/201833051.

A. Burdanov, L. Delrez, M. Gillon, and E. Jehin. Speculoos exoplanet search and its prototype on trappist. *Handbook of Exoplanets*, page 1007–1023, 2018. doi: 10.1007/978-3-319-55333-7_130. URL http://dx.doi.org/10.1007/978-3-319-55333-7_130.

Benoit Carry. Solar system science with esa euclid. *Astronomy and Astrophysics*, 609, 11 2017. doi: 10.1051/0004-6361/201730386.

K. C. Chambers, E. A. Magnier, N. Metcalfe, H. A. Flewelling, M. E. Huber, C. Z. Waters, L. Denneau, P. W. Draper, D. Farrow, D. P. Finkbeiner, C. Holmberg, J. Koppenhoefer, P. A. Price, A. Rest, R. P. Saglia, E. F. Schlafly, S. J. Smartt,

W. Sweeney, R. J. Wainscoat, W. S. Burgett, S. Chastel, T. Grav, J. N. Heasley, K. W. Hodapp, R. Jedicke, N. Kaiser, R. P. Kudritzki, G. A. Luppino, R. H. Lupton, D. G. Monet, J. S. Morgan, P. M. Onaka, B. Shiao, C. W. Stubbs, J. L. Tonry, R. White, E. Bañados, E. F. Bell, R. Bender, E. J. Bernard, M. Boegner, F. Boffi, M. T. Botticella, A. Calamida, S. Casertano, W. P. Chen, X. Chen, S. Cole, N. Deacon, C. Frenk, A. Fitzsimmons, S. Gezari, V. Gibbs, C. Goessl, T. Goggia, R. Gourgue, B. Goldman, P. Grant, E. K. Grebel, N. C. Hambly, G. Hasinger, A. F. Heavens, T. M. Heckman, R. Henderson, T. Henning, M. Holman, U. Hopp, W. H. Ip, S. Isani, M. Jackson, C. D. Keyes, A. M. Koekemoer, R. Kotak, D. Le, D. Liska, K. S. Long, J. R. Lucey, M. Liu, N. F. Martin, G. Masci, B. McLean, E. Mindel, P. Misra, E. Morganson, D. N. A. Murphy, A. Obaika, G. Narayan, M. A. Nieto-Santisteban, P. Norberg, J. A. Peacock, E. A. Pier, M. Postman, N. Primak, C. Rae, A. Rai, A. Riess, A. Riffeser, H. W. Rix, S. Röser, R. Russel, L. Rutz, E. Schilbach, A. S. B. Schultz, D. Scolnic, L. Strolger, A. Szalay, S. Seitz, E. Small, K. W. Smith, D. R. Soderblom, P. Taylor, R. Thomson, A. N. Taylor, A. R. Thakar, J. Thiel, D. Thilker, D. Unger, Y. Urata, J. Valenti, J. Wagner, T. Walder, F. Walter, S. P. Watters, S. Werner, W. M. Wood-Vasey, and R. Wyse. The pan-starrs1 surveys. 12 2016.

C. Chyba and C. Sagan. Endogenous production, exogenous delivery and impact-shock synthesis of organic molecules: an inventory for the origins of life. *Nature*, 355(6356):125–132, January 1992. doi: 10.1038/355125a0.

L. Delrez, M. Gillon, D. Queloz, B.-O. Demory, Y. Almleaky, J. de Wit, E. Jehin, A. H. M. J. Triaud, K. Barkaoui, A. Burdanov, A. J. Burgasser, E. Ducrot, J. Mc-Cormac, C. Murray, C. Silva Fernandes, S. Sohy, S. J. Thompson, V. Van Grootel, R. Alonso, Z. Benkhaldoun, and R. Rebolo. Speculoos: a network of robotic telescopes to hunt for terrestrial planets around the nearest ultracool dwarfs, 2018.

J. Durech, M. Kaasalainen, B. D. Warner, M. Fauerbach, S.A. Marks, S. Fauvaud, M. Fauvaud, J. M. Vugnon, F. Pilcher, L. Bernasconi, and R. Behrend. Asteroid models from combined sparse and dense photometric data. *Astronomy and Astrophysics*, 493(1):291–297, January 2009. doi: 10.1051/0004-6361:200810393.

J. P. Emery, F. Marzari, A. Morbidelli, L. M. French, and T. Grav. The complex history of trojan asteroids. *Asteroids IV*, 06 2015. doi: 10.2458/azu_uapress_9780816532131-ch011.

T.L. Farnham, D. G. Schleicher, and M. F. A'Hearn. The HB Narrowband Comet Filters: Standard Stars and Calibrations. *Icarus*, 147(1):180–204, September 2000. doi: 10.1006/icar.2000.6420.

M. Ferrais. *TRAPPIST Asteroid Lightcurves*. Master thesis, ULiege, 2018.

M. Gillon. Searching for red worlds. *Nature Astronomy*, 2:344–344, April 2018. doi: 10.1038/s41550-018-0443-y.

M. Gillon, Amaury H. M. J. Triaud, B-O Demory, E. Jehin, E. Agol, K. M. Deck, S. M. Lederer, J. de Wit, A. Burdanov, J. G. Ingalls, E. Bolmont, J. Leconte,

S. N. Raymond, F. Selsis, M. Turbet, K. Barkaoui, A. Burgasser, M. R. Burleigh, S. J. Carey, A. Chaushev, C. M. Copperwheat, L. Delrez, C. S. Fernandes, D. L. Holdsworth, E. J. Kotze, V. Van Grootel, Y. Almleaky, Z. Benkhaldoun, P. Magain, and D. Queloz. Seven temperate terrestrial planets around the nearby ultra-cool dwarf star trappist-1, 2017.

P. Guzik, M. Drahus, K. Rusek, W. Waniak, G. Cannizzaro, and I. Pastor-Marazuela. Initial characterization of interstellar comet 2i/borisov. *Nature Astronomy*, 4:53–57, Oct 2019. doi: 10.1038/s41550-019-0931-8.

A. Ivantsov, D. Hestroffer, J. Desmars, W. Thuillot, and P. David. Comparison of PHA's close encounter predictions. In *EPSC-DPS Joint Meeting 2019*, volume 2019, pages EPSC–DPS2019–1883, September 2019.

E. Jehin, M. Gillon, D. Queloz, P. Magain, J. Manfroid, V. Chantry, M. Lendl, D. Hutsemékers, and S. Udry. Trappist: Transiting planets and planetesimals small telescope. *The Messenger*, 09 2011.

E. Jehin, M. Gillon, D. Queloz, L. Delrez, A. Burdanov, C. Murray, S. Sohy, E. Ducrot, D. Sebastian, S. Thompson, J. McCormac, Y. Almleaky, A.J. Burgasser, B. O. Demory, J. de Wit, K. Barkaoui, F.J. Pozuelos, A.H.M.J. Triaud, and V.V. Grootel. The SPECULOOS Southern Observatory Begins its Hunt for Rocky Planets. *The Messenger*, 174:2–7, December 2018. doi: 10.18727/0722-6691/5105.

David Jewitt. The active asteroids. *The Astronomical Journal*, 143:66, 02 2012. doi: 10.1088/0004-6256/143/3/66.

M. Kaasalainen, S. Mottola, and M. Fulchignoni. *Asteroid Models from Disk-integrated Data*, pages 139–150. 2002.

N. Kaiser, W. Burgett, K. Chambers, L. Denneau, J. Heasley, R. Jedicke, E. Magnier, J. Morgan, P. Onaka, and J. Tonry. title>the pan-starrs wide-field optical/nir imaging survey</title. *Proceedings of SPIE - The International Society for Optical Engineering*, 7733:77330E, 07 2010. doi: 10.1117/12.859188.

D. Lowe and G. Byerly. The terrestrial record of late heavy bombardment. *New Astronomy Reviews*, 81, 03 2018. doi: 10.1016/j.newar.2018.03.002.

M. Mahlke, H. Bouy, B. Altieri, G. Verdoes Kleijn, B. Carry, E. Bertin, J. Jong, K. Kuijken, J. McFarland, and E. Valentijn. Mining the kilo-degree survey for solar system objects. *Astronomy and Astrophysics*, 610, 11 2017. doi: 10.1051/0004-6361/201730924.

M. Mahlke, E. Solano, H. Bouy, B. Carry, G. Verdoes Kleijn, and E. Bertin. The ssos pipeline: Identification of solar system objects in astronomical images. *Astronomy and Computing*, 28:100289, Jul 2019. doi: 10.1016/j.ascom.2019.100289.

A. Marciniak, F. Pilcher, D. Oszkiewicz, T. Santana-Ros, S. Urakawa, S. Fauvaud, P. Kankiewicz, Ł. Tychoniec, M. Fauvaud, R. Hirsch, J. Horbowicz, K. Kamiński, I. Konstanciak, E. Kosturkiewicz, M. Murawiecka, J. Nadolny, K. Nishiyama,

S. Okumura, M. Polińska, F. Richard, T. Sakamoto, K. Sobkowiak, G. Stachowski, and P. Trela. Against the biases in spins and shapes of asteroids. *Monthly Notices of the Royal Astronomical Society*, 118:256–266, December 2015. doi: 10.1016/j.pss.2015.06.002.

J. L. Margot, P. Pravec, P. Taylor, B. Carry, and S. Jacobson. *Asteroid Systems: Binaries, Triples, and Pairs*, pages 355–374. 2015. doi: 10.2458/azu_uapress_9780816532131-ch019.

K. Meech, R. Weryk, M. Micheli, J. Kleyna, O. Hainaut, R. Jedicke, R. Wainscoat, K. Chambers, J. Keane, A. Petric, L. Denneau, E. Magnier, T. Berger, M. Huber, H. Flewelling, C. Waters, E. Schunova-Lilly, and S. Chastel. A brief visit from a red and extremely elongated interstellar asteroid. *Nature*, 552, 12 2017. doi: 10.1038/nature25020.

M. Mommert. Photometrypipeline: An automated pipeline for calibrated photometry. *Astronomy and Computing*, 18:47–53, Jan 2017. ISSN 2213-1337. doi: 10.1016/j.ascom.2016.11.002.

Filipe Monteiro, José Sergio Silva, Francisco Tamayo, Teresinha Rodrigues, and Daniela Lazzaro. Shape model and spin direction analysis of PHA (436724) 2011 UW158: a large superfast rotator. *Monthly Notices of the Royal Astronomical Society*, 495(4):3990–4005, May 2020. doi: 10.1093/mnras/staa1401.

NASA/JPL. Asteroids, a. URL https://ssd.jpl.nasa.gov/?asteroids. Accessed: 2020-07-02.

NASA/JPL. Comets, b. URL https://ssd.jpl.nasa.gov/?comets. Accessed: 2020-07-02.

D. P. O'Brien and R. Greenberg. The collisional and dynamical evolution of the main-belt and NEA size distributions. *Icarus*, 178:179–212, November 2005. doi: 10.1016/j.icarus.2005.04.001.

F. Ochsenbein, P. Bauer, and J. Marcout. The VizieR database of astronomical catalogues. *Astronomy and Astrophysics Supplement*, 143:23–32, April 2000. doi: 10.1051/aas:2000169.

J. Ortiz, B. Sicardy, F. Braga-Ribas, A. Alvarez-Candal, E. Lellouch, R. Duffard, N. Pinilla-Alonso, V. Ivanov, S. Littlefair, J. Camargo, M. Assafin, E. Unda-Sanzana, E. Jehin, N. Morales, G. Tancredi, R. Gil-Hutton, I. Cueva, J. Colque, D. Neto, and M. Emilio. Albedo and atmospheric constraints of dwarf planet makemake from a stellar occultation. *Nature*, 491:566–9, 11 2012. doi: 10.1038/nature11597.

R. E. Pike, S. Lawler, R. Brasser, C. J. Shankman, M. Alexandersen, and J. J. Kavelaars. The structure of the distant kuiper belt in a nice model scenario. *The Astronomical Journal*, 153:127, Feb 2017. doi: 10.3847/1538-3881/aa5be9.

T. Prusti, J. H. J. de Bruijne, A. G. A. Brown, A. Vallenari, C. Babusiaux, C. A. L. Bailer-Jones, U. Bastian, M. Biermann, D. W. Evans, and et al. The gaia mission. *Astronomy and Astrophysics*, 595:A1, Nov 2016. doi: 10.1051/0004-6361/201629272.

M. Rosing and R. Frei. U-rich archaean sea-floor sediments from greenland – indications of >3700 ma oxygenic photosynthesis. *Earth and Planetary Science Letters*, 217:237–244, 01 2004. doi: 10.1016/S0012-821X(03)00609-5.

P. M. B. Shames and Tody D. *A User's Introduction to the IRAF Command Language - Version 2.3*, 1986.

B. Sicardy, J. Ortiz, M. Assafin, E. Jehin, A. Maury, E. Lellouch, R. Gil-Hutton, F. Braga-Ribas, F. Colas, D. Hestroffer, J. Lecacheux, F. Roques, P. Santos-Sanz, T. Widemann, N. Morales, R. Duffard, A. Thirouin, A. Castro-Tirado, M. Jelínek, and H. Hernández-Toledo. A pluto-like radius and a high albedo for the dwarf planet eris from an occultation. *Nature*, 478:493–6, 10 2011. doi: 10.1038/nature10550.

T. Spohn, D. Breuer, and T. V. Johnson, editors. Elsevier, Boston, 2014. doi: https://doi.org/10.1016/C2010-0-67309-3. URL http://www.sciencedirect.com/science/article/pii/B9780124158450050015.

E. F. Tedesco and F-X Desert. The [ITAL]infrared space observatory[/ITAL] deep asteroid search. *The Astronomical Journal*, 123:2070–2082, apr 2002. doi: 10.1086/339482.

Minor Planet Center. New- and old-style minor planet designations. URL https://minorplanetcenter.net//iau/info/OldDesDoc.html. Accessed: 2020-07-25.

Minor Planet Center. Plot of the inner solar system, 2019a. URL https://minorplanetcenter.net/iau/lists/InnerPlot.html. Accessed: 2020-08-03.

Minor Planet Center. Plot of the outer solar system, 2019b. URL https://minorplanetcenter.net/iau/lists/OuterPlot.html. Accessed: 2020-08-03.

NASA/JPL Center for Near Earth Object Studies. Neo basics. URL https://cneos.jpl.nasa.gov/about/neo_groups.html. Accessed: 2020-08-03.

NASA/JPL Center for Near Earth Object Studies. Discovery statistics, 2020. URL https://cneos.jpl.nasa.gov/stats/totals.html. Accessed: 2020-08-03.

R. Wainscoat, K. Chambers, E. Lilly, R. Weryk, S. Chastel, L. Denneau, and M. Micheli. The pan-starrs search for near earth objects. *Proceedings of the International Astronomical Union*, 10:293–298, 08 2015. doi: 10.1017/S1743921315009187.

K. J. Walsh. Rubble pile asteroids. *Annual Review of Astronomy and Astrophysics*, 56(1):593–624, Sep 2018. doi: 10.1146/annurev-astro-081817-052013.

B. D. Warner, A. W. Harris, and P. Pravec. The asteroid lightcurve database. *Icarus*, 202:134–146, July 2009. doi: 10.1016/j.icarus.2009.02.003.